Icarus 218 (2012) 247–261

Contents lists available at SciVerse ScienceDirect

Icarus

journal homepage: www.elsevier.com/locate/icarus

Optical constants of Titan tholins at mid-infrared wavelengths (2.5–25 μm) and the possible chemical nature of Titan's haze particles

Hiroshi Imanaka [a,b,*], Dale P. Cruikshank [c], Bishun N. Khare [d,b], Christopher P. McKay [e]

[a] Lunar and Planetary Laboratory, University of Arizona, P.O. Box 210092, 1629 E. University Boulevard, Tucson, AZ 85721, United States
[b] SETI Institute, 189 North Bernardo Avenue, Suite 100, Mountain View, CA 94043, United States
[c] NASA Ames Research Center, MS 245-6, Moffett Field, CA 94035, United States
[d] NASA Ames Research Center. MS 239-11, Moffett Field, CA 94035, United States
[e] NASA Ames Research Center, MS 245-3, Moffett Field, CA 94035, United States

ARTICLE INFO

Article history:
Received 6 September 2011
Revised 26 October 2011
Accepted 16 November 2011
Available online 6 December 2011

Keywords:
Titan
Spectroscopy
Organic chemistry
Infrared observations

ABSTRACT

Complex organic materials may exist as haze layers in the atmosphere of Titan and as dark coloring agents on icy satellite surfaces. Laboratory measurements of optical constants of plausible complex organic materials are necessary for quantitative evaluation from remote sensing observations, and to document the existence of complex organic materials in the extraterrestrial environments. The recent Cassini VIMS and CIRS observations provide new constraints on Titan's haze properties in the mid-infrared wavelength region. Here, we present the optical constants (2.5–25 μm) of Titan tholins generated with cold plasma irradiation of a N_2/CH_4 (90/10) gas mixture at pressures of 0.26 mbar, 1.6 mbar, and 23 mbar. Our new optical constants of three types of Titan tholins suggest that no single Titan tholin in this study fulfills all the observational constraints of the Titan haze material. The discrepancy remains a challenge for future modeling and laboratory efforts that aim toward a better understanding of Titan's haze material.

1. Introduction

Complex organic material exists in Titan's atmosphere as haze particles (Waite et al., 2009) and probably on Titan's surface (Soderblom et al., 2009). Furthermore, complex organic materials might exist on the surfaces of outer Solar System bodies and act as coloring agents in visible spectral region (Cruikshank et al., 2005). The determination of optical constants of complex organics produced in laboratory simulations of planetary environments is useful to confirm the existence of complex organic materials in the extraterrestrial environments, and are necessary for quantitative evaluation of remote sensing observations.

Recent Titan observations by the Cassini Visual and Infrared Mapping Spectrometer (VIMS) and the Composite Infrared Spectrometer (CIRS) have revealed spectral features from Titan's haze covering mid-infrared (mid-IR) wavelengths (2.5–25 μm) (de Kok et al., 2007; Bellucci et al., 2009; Rannou et al., 2010; Vinatier et al., 2010; Anderson and Samuelson, 2011). This mid-IR region possesses rich information on chemical functional groups. Thus, reliable optical constants of the class of possible complex organic materials that are produced in laboratory simulations of Titan's atmosphere, conventionally named Titan tholins, would be useful to identify or to quantitatively constrain the chemical structures of such materials. Titan's haze also plays important roles in the radiative balance as an absorber of both solar radiation in visible wavelengths and radiation from Titan's troposphere/surface in the thermal infrared region (McKay et al., 1989, 1991). Thus, optical constants of Titan tholins in the mid-IR region might help develop a better understanding of the radiative balance and dynamics in the atmosphere of Titan.

Only a few quantitative studies have been conducted for the determination of optical constants of Titan tholins or related complex organic materials at the mid-IR wavelengths. Khare et al. (1984) conducted a thorough study of optical constants of a Titan tholin at wavelengths from soft X-ray to microwave frequencies. Since then, several studies of optical constants of Titan tholins have been conducted at visible and near-IR wavelengths (Ramirez et al., 2002; Tran et al., 2003; Imanaka et al., 2004; Vuitton et al., 2009; Hasenkopf et al., 2010). However, in the mid-IR spectral region, the optical constants of the Titan tholin by Khare et al. (1984) have served as the only source for modeling optical properties of Titan's haze at altitudes higher than where the condensates of simple molecules dominate (McKay et al., 2001).

Recent Cassini observations show some discrepancy between the observed extinction features of Titan's haze at 3 μm, 3.4 μm, and around 13–17 μm and the optical constants of the Titan tholin

* Corresponding author at: Lunar and Planetary Laboratory, University of Arizona, P.O. Box 210092, 1629 E. University Boulevard, Tucson, AZ 85721, United States.
E-mail address: himanaka@lpl.arizona.edu (H. Imanaka).

0019-1035/$ - see front matter © 2011 Elsevier Inc. All rights reserved.
doi:10.1016/j.icarus.2011.11.018

as determined by Khare et al. (1984). Bellucci et al. (2009) and Rannou et al. (2010) demonstrated the prominent absorption bands around 3.4 μm, which are absent in the Khare et al. (1984) optical constants. In addition, Vinatier et al. (2010) pointed out that the increase of haze optical depth from 600 to 750 cm^{-1} by a factor of 3 is not consistent with Khare et al. (1984) optical constants. Since the chemical, and thereby optical properties, of Titan tholins depend on the experimental conditions (Imanaka et al., 2004; Cruikshank et al., 2005; Bernard et al., 2006; Quirico et al., 2008), it would be of interest to determine the optical constants for several representative classes of Titan tholins.

The goal of this study is to provide reliable sets of optical constants of Titan tholins in the mid-IR wavelengths (2.5–25 μm) with high spectral resolution and conservative uncertainties. Since Imanaka et al. (2004) and Cruikshank et al. (2005) demonstrated that Titan tholins generated with cold plasma irradiation show a transition from a nitrogen-rich aromatic structure to a less-nitrogenated aliphatic structure with the deposition pressure, we focus on three types of tholins generated at pressures of 0.26 mbar, 1.6 mbar, and 23 mbar. The plasma chemistry at these experimental pressures may not precisely represent the Titan atmospheric chemistry at the corresponding altitudes, but may to some degree exhibit common chemical processes in Titan's upper atmosphere where haze production is occurring (Imanaka and Smith, 2007, 2010; Waite et al., 2007; Gautier et al., 2011; Lavvas et al., 2011). These laboratory materials show wide variations in the optical absorption properties at UV/Vis wavelengths (Imanaka et al., 2004), and probably serve, at least partially, as potential complex organic materials representative of Titan haze materials.

2. Experimental and measurement conditions

Titan tholins were produced in our laboratory with a parallel-plane inductively coupled cold plasma irradiation from a premixed N_2/CH_4 = 10/90 gas mixture (Matheson, Research Grade) at three different pressures, 0.26 mbar (LP samples), 1.6 mbar (MP samples) and 23 mbar (HP sample). The 13.5 MHz RF power of 100 W was used for all experiments in this study. The detailed experimental setup is described in our previous work (Imanaka et al., 2004). Thin film samples were deposited on substrates, such as KBr, CaF_2, and UV-grade quartz substrates (25 mm diameter with 2 mm thickness). In order to generate thin films with various thicknesses (ranging between 0.5 μm and 10 μm), the experiments were repeated for different durations. Table 1 summarizes the experimental conditions.

The films deposited on substrates were characterized with a prism coupler (Metricon, Model 2010) and with a single-beam FT-IR spectrometer (Nicolet, Nexus 670) (Fig. 1). The prism coupler (Metricon, Model 2010) can measure refractive index, n, with accuracy better than 0.0005, described in Section 3. We employed two laser wavelengths at 1.547 μm and 0.637 μm. Transmittance and reflectance of the tholin film and substrate systems were measured in the wavelength region 1.47–25 μm (7000–400 cm^{-1}) with spectral resolution 0.5 cm^{-1}. The transmittance was measured at the normal angle, and the reflectance was measured at near normal angle (11°) by using a gold mirror as a reference. For several samples, only the transmittance was measured, as shown in Table 1. Optical constants and thicknesses were determined by a two-step iterative procedure for fitting the observed transmittance and reflectance (Fig. 1), which is described in Section 4. The optically determined thickness of each sample is also listed in Table 1.

3. Refractive indices (n) at 1.547 μm and 0.637 μm and mass density of Titan tholins

The prism coupling technique is a proven technique to measure the thickness and real part of the complex refractive index (n) of dielectric and polymer films by observing the wave guiding modes of the sample (Kersten, 1975; Adams et al., 1979; Sharda et al., 2003). The sample is brought into contact with the base of a prism by means of a pneumatically-operated coupling head, creating a small air gap between the film and the prism. A laser beam strikes the base of the prism, and the reflection is measured by a photodetector as a function of the incident angle of the laser beam (Fig. 1). When the photon enters into a guided optical propagation mode at certain incident angles, the reflected light shows a sharp decrease in its intensity. It is essential that the angle of such sharp peak is accurately determined, but the measurement of the absolute reflected intensity is not an issue. The accuracies of the thickness and refractive index measurements (Metricon, Model 2010) are typically less than 1% and ±0.0005, respectively.

For independent measurement of thickness and refractive index, film thickness must be sufficient to support two or more guided modes. The typical thickness of Titan tholin for the reliable measurements in this study turns out to be in the range of 1.5–10 μm. Furthermore, absorption of the film is required to not be too large for measuring the sharp decrease in reflected intensity. The measurements conducted at laser wavelength 1.547 μm were particularly good for substantially thick samples in our study. Table 2 shows the summary of the prism coupling measurements.

One of the LP samples generated at 0.26 mbar (Run 25) visually showed apparent inhomogeneity. The laser irradiated several spots in the same film to examine the inhomogeneity. These

Table 1
Summary of experimental and measurement conditions.

Pressure	Run #	Duration (h)	Substrate	IR spectra	Thickness (μm)
p = 0.26 mbar (LP)	Run 25	9	KBr	T and R	6.6 ± 0.5
	Run 07	1	CaF_2	T	0.707 ± 0.005
	Run 01	5	KBr	T	4.25 ± 0.05
	Run 82	65			
p = 1.6 mbar (MP)	Run 24	9	KBr	T and R	11.14 ± 0.023
	Run 40	3	CaF_2	T and R	2.057 ± 0.008
	Run 09	3	CaF_2	T	2.45 ± 0.01
	Run 04	1	KBr, CaF_2	T	0.92 ± 0.05
	Run 18	9	KBr	T	11.0 ± 1.0[a]
	Run 87	31			
p = 23 mbar (HP)	Run 13	3	KBr, (Qz)	T	2.2 ± 1.2[b]
	Run 23[c]	9	(Qz)		4.8 ± 0.5[a]

All samples are generated from plasma irradiation (13 MHz, 100 W) of a N_2/CH_4 = 90/10 gas mixture.
[a] Rough thickness only estimated from stylus measurements and a prism coupling technique.
[b] Thickness estimated from a sample on quartz (Qz) substrate.
[c] During the Run 23, the pressure accidentally reduced to a few mbar for approximately 4 h.

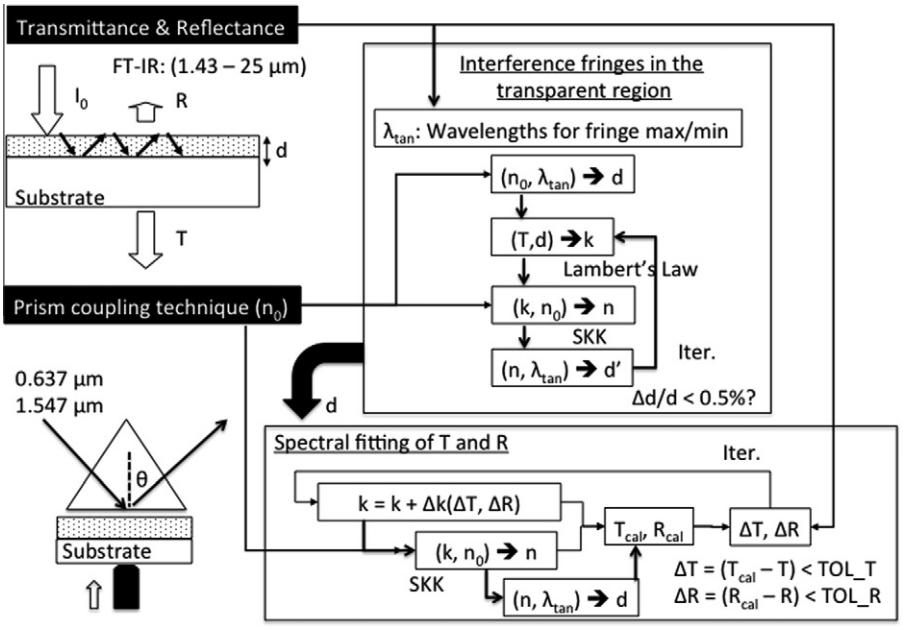

Fig. 1. Measurements and analytical method in this study. See the main text.

Table 2
The refractive index (n) and thickness of Titan tholins at two different wavelengths measured with a prism coupling technique.

Sample			0.637 μm		1.547 μm	
Run #	Pressure (mbar)	Substrate	n	Thickness (μm)	n	Thickness (μm)
Run 25	0.26	Qz	1.627	4.61		
			1.637	5.67		
			1.631	4.96		
					1.600	5.38
			1.634	6.96	1.589	6.94
Run 82	0.26	Glass slide	1.645[a]		1.606[a]	38.8[b]
Run 24	1.6	Qz	1.586	11.27	1.563	11.17
Run 18	1.6	KBr	1.582		1.568	12.22
Run 23	23	Qz	1.574	5.39		
					1.554	4.30

[a] Critical angle measurements.
[b] Based on the assumption of n determined by a critical angle measurement.

measurements showed slight inhomogeneity in n, but the visual inhomogeneity was dominated by the difference in thickness (Table 2). Two samples in different runs (Run 24 and Run 18) demonstrated only slight differences in the measured n values (Table 2). This inhomogeneity gives an estimate of the uncertainty in n-values of our tholin samples. The real part of refractive indices at 1.547 μm for those two type of tholins are constrained as $n = 1.600 \pm 0.001$ for the LP samples and $n = 1.566 \pm 0.003$ for the MP samples. Unfortunately, we only have one measurement for the HP sample, and $n = 1.554$ was obtained at 1.547 μm. This particular HP sample (Run 23), however, should be treated as intermediate between the MP sample and the HP sample because of an accidental drop in deposition pressure (Table 1).

It has been known for some time that the refractive index (n) of hydrogenated amorphous carbon generally correlates with its mass density, ρ (Dischler and Bayer, 1990; Ferrari et al., 2000). Refractive indices (n) of dielectric materials are, to a first approximation, related to molecular polarizability and their densities by the Lorentz–Lorenz relation (Born and Wolf, 1997). Assuming that molecular refractivity and molecular weight are independent, the Lorentz–Lorenz coefficient, $[(n^2-1)/(n^2+2)]/\rho$, is independent of phase where absorption, k, is extremely small (Robertson et al., 1975). The bulk mass density of the tholin samples scratched off from the substrate were measured with a pycnometer (ACCUPYC 1330 at Micrometrics) as 1.3866 ± 0.0004 (g/cm^3) for the LP tholin (Run 82) and 1.3113 ± 0.0003 (g/cm^3) for the MP tholin (Run 87). The LP tholin and MP tholin are not exactly the same chemical structures and may not be applicable for the assumptions above. Nonetheless, it is interesting that the Lorentz–Lorenz coefficients for both tholins are coincident within 1%. The dominant building blocks, carbon and probably nitrogen networks, of these tholins might possess many common skeletal structures. If this Lorentz–Lorenz coefficient still holds for the HP tholins, its mass density would be approximately 1.28 g/cm^3. These mass densities of the Titan tholins can also be used to calculate mass extinction coefficients (cm^2/g) not only for comparison with laboratory data for hydrogenated amorphous carbons prepared for astronomical interests (Furton et al., 1999; Mennella et al., 2002), but also for estimation of the aerosol mass load in the Titan atmosphere.

4. Determination of optical constants (n and k)

Fig. 2 shows examples of measured transmittance and reflectance of a tholin film deposited on a substrate. A calibration of transmittance and reflectance is conducted by measuring several different substrates as standards under the same optical conditions.

The theoretical transmittance and reflectance can be calculated for those standards with known complex refractive indices (Palik, 1991), and the possible systematic errors caused by the instrumental responses are removed to obtain the absolute transmittance and reflectance of the film and substrate system. Random noise in transmittance and reflectance is substantially larger near the edge of our measurements (Fig. 2), but typically lower than 0.0005 for transmittance and 0.005 for reflectance at wavelengths between 2.5 and 20 μm (4000–500 cm^{-1}).

In order to obtain reliable optical constants ($n + ik$), the film thickness (d) has to be determined as accurately as possible. We assumed a simple geometry of the film and substrate system as a smooth, parallel, and homogenous film. Under this approximation, we conducted an iterative subtractive Kramers–Kronig (SKK) analysis for determining a self-consistent set of optical constants and thickness, as shown in Fig. 1. The well constrained n-values in the near-IR region (1.547 μm), as described in Section 3, have two major benefits in conducting such an iterative SKK analysis; (1) the film thickness can be accurately ($\lesssim$1%) determined from the observed interference fringes in a transparent region (1.43–2.5 μm), and (2) the real part, n, can be well constrained by the SKK analysis using an accurate anchor point at 1.547 μm.

Whenever interference fringes are observable in the near-IR region, the fringe positions of maxima and minima (tangential wavelengths, λ_{tan}) are obtained. Assuming $n(\lambda)$ as a constant at the value obtained at 1.547 μm with the prism coupler, the thickness of the film can be initially estimated by determining the interference order, m,

$$2n_{tan}d = m\lambda_{tan}. \quad (1)$$

The refractive index of tholin film around at 1.547 μm (Table 2) is greater than that of KBr and CaF_2 substrates (Palik, 1991), so that the interference order, m, should be exact integers at the fringe maxima in transmittance and fringe minima in reflectance (Swanepoel, 1983). Using the estimated thickness, approximate $k(\lambda)$ values can be obtained from Lambert's law where tholins are optically thick enough ($kd \sim \lambda/4\pi$),

$$k = \frac{\lambda}{4\pi d}\ln\frac{(1-R)}{T}. \quad (2)$$

The wavelength dependence of n can be obtained by a subtractive Kramers–Kronig analysis (Ahrenkiel, 1971; Hawranek et al., 1976; Wood and Roux, 1982; Masterson and Khanna, 1990; Toon et al., 1994),

$$n(\nu) = n_0 + \frac{2(\nu^2-\nu_0^2)}{\pi}P\int_0^\infty \frac{\nu' k(\nu')}{(\nu'^2-\nu^2)(\nu'^2-\nu_0^2)}d\nu'. \quad (3)$$

Here, ν represents wavenumber (cm^{-1}). The above Cauchey's principal value should be integrated for the entire range of all wavelengths. However, in practice, it is only integrated over a limited wavelength interval. The anchor point, n_0, at 1.547 μm (corresponding to ν_0) reduces the effect of the above numerical integration in a limited spectral range (1.43–25 μm), especially for the cut-off at the shorter wavelength. At wavelengths longer than our measurement range, k is assumed to be constant as the values at the longest observed wavelength. This assumption in the SKK integral is generally valid unless a large local absorption peak exists just outside our measurement range. For estimating n from the Kramers–Kronig relation, the effect of very weak absorption features with small k has negligible effect. Therefore, the above mentioned optically thick approximation of k can provide reasonable dispersion relation of $n(\lambda)$ in the near-IR range. Using this dispersion of $n(\lambda)$, the thickness can be updated to match all the observed tangential wavelengths with exact interference orders (Swanepoel, 1983; Wang and Miyagi, 1997).

Once the film thickness is accurately determined within ~0.5%, the optical constants are finely tuned by fitting the observed transmittance (T) and reflectance (R) by comparing the calculated transmittance and reflectance. The synthetic transmittance (T_cal) and reflectance (R_cal) can be calculated by using rigorous formulas for a film on a finite thickness substrate including effects of coherent multiple reflection inside the film and incoherent multiple reflection inside the substrate (Harbecke, 1986; Stenzel et al., 1991) (Appendix A). The convergence conditions are that the difference of those observed T and R from the synthetic T_cal and R_cal are within the tolerance. The tolerance is set to the random noise of T and R. However, if no convergence is obtained due to possible systematic errors, the tolerance is set to a larger value. This results in a fitting residual larger than random noise. Both the random noise and the fitting residual are considered in the error propagation to estimate uncertainties in the determined optical constants. Calculated transmittance and reflectance using the thickness and optical constants of the film show reasonable match to the observed values as shown in Fig. 2.

This two-step iterative procedure allows us to determine optical constants of each tholin sample across mid-IR wavelengths. Fig. 3 shows examples of the derived optical constants for the Titan tholin generated at 1.6 mbar with different film thicknesses. For a sample deposited on a CaF_2 substrate, the analysis is only conducted at wavelengths between 1.43 and 7.41 μm (7000–1350 cm^{-1}) (Fig. 3b).

The dependence of the optical constants on experimental uncertainties can be estimated by considering the error propagation of the uncertainties of T, R, and thickness, as described in Appendix A. Those uncertainties are also shown in Fig. 3. The uncertainty of k (Fig. 3a, 11.14 (±0.02) μm sample) is typically smaller than 1% where k is larger than 0.05, but increases to 10%,

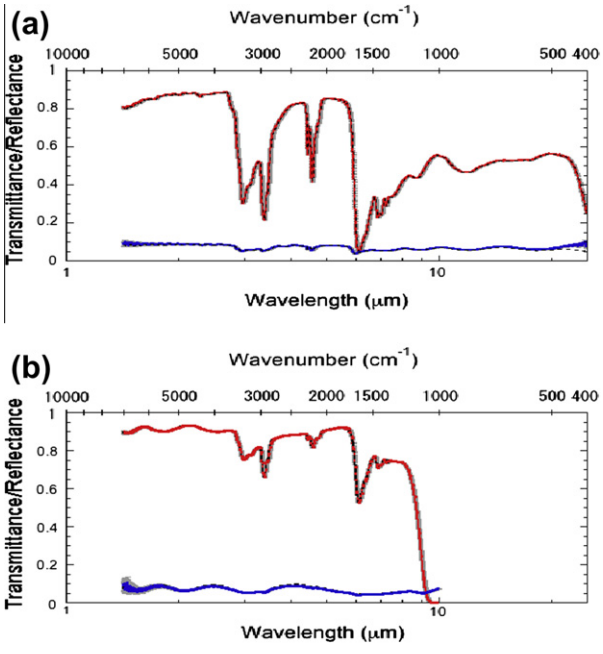

Fig. 2. Typical transmittance and reflectance spectra of Titan tholins measured in the wavelength range of 1.43–25 μm (7000–400 cm^{-1}) are shown in red and blue lines, respectively. The random errors are shown in gray. The calculated transmittance and reflectance using a set of derived optical constants are shown as dashed lines. (a) Titan tholin (1.6 mbar, 9 h) deposited on a KBr substrate. (b) Titan tholin (1.6 mbar, 3 h) deposited on a CaF_2 substrate. Notice that the interference fringes observed in 1.43–3 μm regions are reasonably fitted. (For interpretation of the references to color in this figure legend, the reader is referred to the web version of this article.)

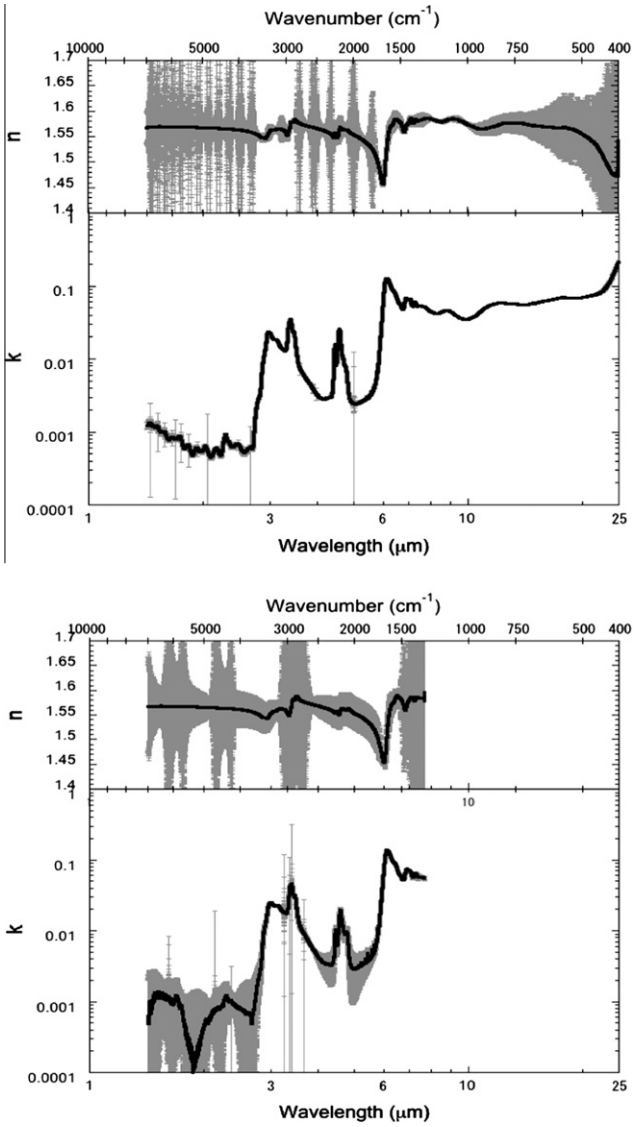

Fig. 3. Example of optical constants of Titan tholins derived from (a) Titan tholin (1.6 mbar, 9 h) deposited on a KBr substrate and (b) Titan tholin (1.6 mbar, 3 h) deposited on a CaF_2 substrate. The uncertainty of optical constants is shown in gray.

where k is smaller than 0.05. As expected, for the thinner sample of 2.06 (±0.01) μm (Fig. 3b), the uncertainty in k becomes much larger. However, it remains within a few % where k is larger than 0.01. Thus, as long as the thickness is determined with accuracy within 1%, those k values larger than 0.01 can be determined with uncertainty less than a few % in our experimental conditions.

On the contrary, the uncertainty in n is apparently widely dispersed. The periodic burst of uncertainty in n-values is because of the singularity where the optical constants become insensitive to the transmittance and reflectance containing finite measurement errors. This singularity has been thoroughly described in past literature (e.g., del Pozo and Díaz, 1992). Except for such bursts, the uncertainty of n can be up to 0.05–0.1, especially near the edge of our measurement wavelength region. This large uncertainty is primarily because of the fitting residual and uncertainty of reflectance. Furthermore, our samples show a slight departure from a perfect specular/parallel film, and the measurement spots of transmittance and reflectance are not exactly the same. These factors probably cause such large uncertainty in n.

The above uncertainty of n does not reflect any physical constraints, but is simply estimated from uncertainties in the transmittance and reflectance. However, we put a constraint on n using the fundamental physical relations of the Kramers–Kronig analysis with a help of an anchor point. Thus, the uncertainty in n should be determined from error propagations of the accuracy of n at the anchor point (less than 0.01 as described in Section 3) and in the Kramers–Kronig integration of $k(\lambda)$. An estimation of the error propagation of the Kramers–Kronig integration from $k(\lambda)$ is not a simple task (Ohta and Ishida, 1988). Furthermore, the assumption of $k(\lambda)$ as constant at the longer wavelengths outside our measurement range potentially compromises the $n(\lambda)$ near the edge (~10–25 μm) of our measurement range. Since $k(\lambda)$ are reasonably constrained with smooth variations and n is measured accurately at 1.547 μm, we believe that the reasonable uncertainty of $n(\lambda)$ is less than 0.01 at wavelengths shorter than 10 μm, except at ~6 μm where n demonstrates a deep minimum because of intense absorption at the same wavelength. This uncertainty would be more realistic than the large error bars shown in Fig. 3.

We experienced some difficulties in the LP tholin samples to generate uniform/parallel but sufficiently thick samples (>5–10 μm) on a KBr substrate with our apparatus. The departure from the ideal parallel film reduces or even obscures the observation of multiple interference fringes in our measurement ranges. (For samples thinner than 2 μm, it was easy to observe interference fringes in transmittance.) Thus, the optical determination of thickness contains large uncertainties (6.6 ± 0.5 μm for Run 25 sample). Such imperfections in the thin film result in uncertainties in the optical constants determined, especially where optically thin.

Finally, we comment on the analysis using only a transmittance spectrum. The iterative SKK analysis has been used for determination of optical constants of pure ice components only from transmittance spectra (Wood and Roux, 1982; Masterson and Khanna, 1990; Pearl et al., 1991; Toon et al., 1994; Moore et al., 2010). If interference fringes are observed in our transmittance spectrum or an estimation of thickness is given from a different measurement, the above approach is also possible for our tholin samples. Fitting only transmittance is very easy, and the uncertainty of n and k is mostly dominated by the uncertainty of thickness estimation. Those uncertainties are much smaller in comparison to that estimated from both transmittance and reflectance. However, such uncertainty would be too small unless they are independently checked with samples of multiple thicknesses, as done in Toon et al. (1994). We describe this issue in the next section.

5. Optical constants for three types of Titan tholins in the mid-IR wavelengths

Fig. 4 shows all the optical constants of Titan tholins generated at 0.26 mbar and 1.6 mbar determined independently from each sample. The optical constants obtained with different thicknesses are very consistent, except at wavelengths longer than 10 μm. This excellent consistency of k-values larger than 0.005 confirms that our assumption of simple film geometry is reasonable for those large k-values. Those k-values smaller than 0.005 can be affected by multiple causes, such as possible scattering loss, a slightly tilted sample, and background instability. The effect of surface scattering loss generally shows a larger effect in shorter wavelengths. Such a tendency is only seen in our thickest sample (Run 24 and Run 25) at wavelengths shorter than 1.5–2 μm. Examination of surface roughness with a SEM (scanning electron microscope) and an AFM (atomic force microscope) demonstrated that the surface roughness, σ, is less than 40 nm in those samples. We confirmed that such nanoscale random roughness has a negligible effect in the mid-IR wavelength region (2.5–25 μm), because the scattering loss decreases toward longer wavelengths following $\exp[-(\sigma/\lambda)^2]$ (Beckmann and Spizzichino, 1963). As described in the previous

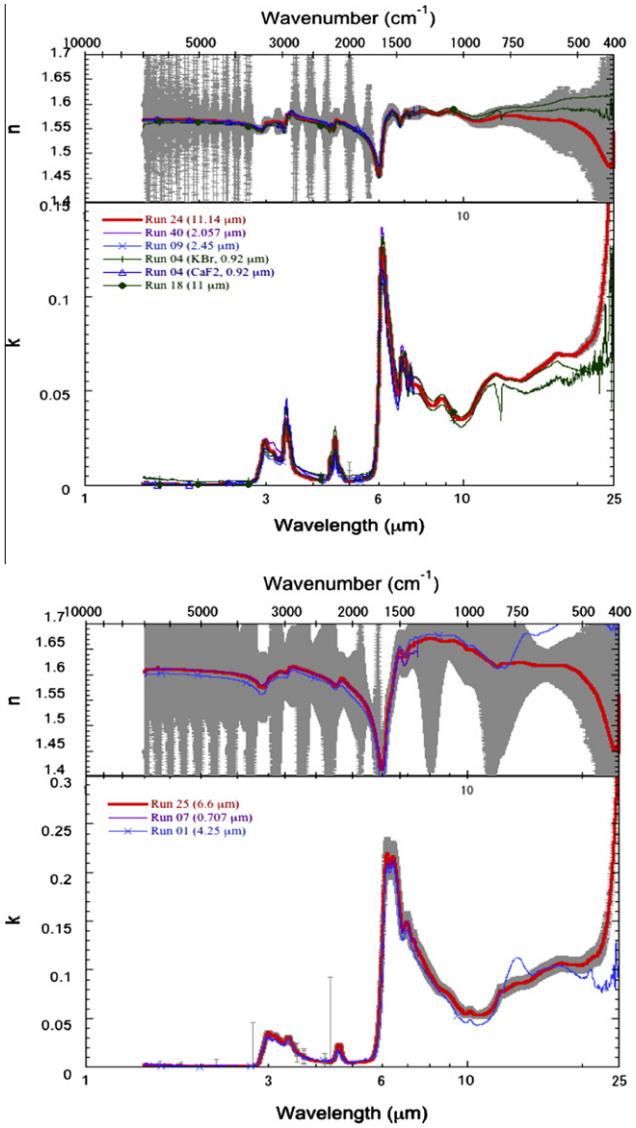

Fig. 4. Optical constants of tholins independently derived from tholin films with different thicknesses. Five different samples generated at 1.6 mbar (upper panel) and three different samples generated at 0.26 mbar (lower panel). For clarity, only the uncertainties for the thickest samples (Run 24 and Run 25) are shown in gray.

section, for thick samples (5–10 μm), the slight tilt of the film within the measurement spot can be the dominant source of systematic errors. This has potential impact on the derived *k*-values especially at wavelengths where the sample is optically thin, but has a negligible effect on large *k*-values. Sudden fluctuations or long term drift of light intensity in our FT-IR spectrometer could also cause systematic errors in absolute transmittance and reflectance, but this is difficult to evaluate at this point. We did not use any artificial background correction, therefore the derived *k*-values less than 0.01 should be considered as an upper limit at the present time.

A systematic inhomogeneity within a film cannot be fully excluded even though our parallel-plane inductively coupled plasma apparatus is designed for homogenous deposition in a wide area. The possible spatial variation of plasma properties, such as electron density and electron temperature, might result in the systematic variation of optical constants within a film. However, such effect is already included in the above uncertainties because of reasonable agreements in the derived *k*-values from different experimental runs.

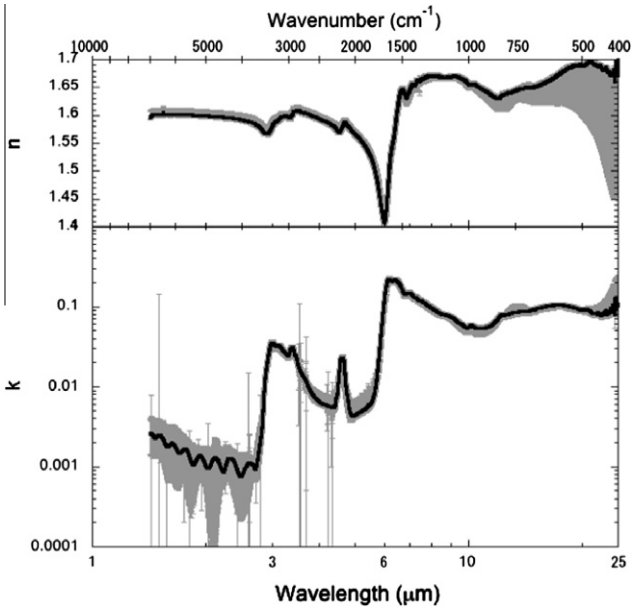

Fig. 5. Optical constants of Titan tholins generated with cold plasma irradiation of a $N_2/CH_4 = 90/10$ gas mixture at 0.26 mbar (LP). The imaginary part of complex reflective indices, *k*, at wavelength less than 2.7 μm should be treated only as upper limits because of possible departure of analyzed films from an ideal parallel plane/smooth case.

As described in the previous section, our methodology of iterative SKK analysis with an accurate anchor point allows much tighter constraints on $n(\lambda)$ than those estimated simply from error propagation of the uncertainties of *T* and *R*. In fact, the derived *n*-values from various samples match extremely well (within 1%). This is because of the good match in our derived *k*-values, especially for *k* larger than 0.005. We believe that the derived *n*-values are accurate to better than 1% at least for wavelengths less than 10 μm. The sample on the CaF_2 substrate was only analyzed at wavelengths shorter than 7.5 μm. Our assumption of constant *k* outside of the measurement range (>7.5 μm) has little effect on *n*-values, even with slight departures of the assumed constant *k* from the derived *k*-values for the samples on the KBr substrates. The *n*-values between 20 and 25 μm are probably not well constrained at this moment. This is partially because of the apparent absorption at the edge in the above measurement (Run 24 sample). The wavelength cut-off of the KBr substrate and possible systematic error in this region probably causes such uncertainty, however, the exact reason is not known at this moment.

Because of the fact that independently derived *k*-values reasonably match each other, especially for large *k*, we can select the *k*-values determined from thickest samples as representative for the Titan tholins under each experimental condition. In the wavelength region longer than 10 μm, *k*-values show slight discrepancies that should be treated as uncertainty. As described above, an absorption feature toward the edge of our measurement range sometimes shows up at wavelengths 20–25 μm. This apparent absorption has substantial effects in *n* for wavelengths longer than 10 μm. However, those apparent peaks are not observed for all runs, and we therefore chose the *k*-values without such apparent absorption. This omission is also consistent with the recent reflectance measurements of a Titan tholin that shows no such strong absorption features near 400 cm^{-1} (Brucato et al., 2010). We conducted a final SKK analysis using the composite $k(\lambda)$ to obtain $n(\lambda)$. Figs. 5 and 6 show the optical constants of Titan tholins generated at 0.26 mbar and 1.6 mbar.

This set of optical constants is used for a final error estimation by comparing all available transmittance and reflectance

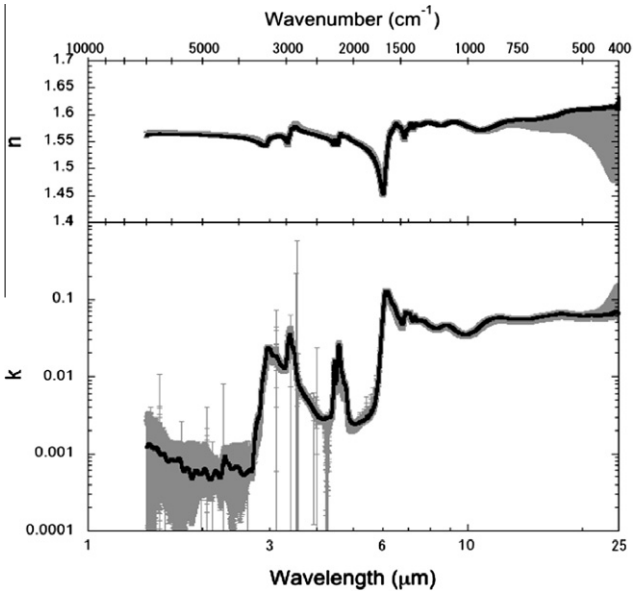

Fig. 6. Optical constants of Titan tholins generated by cold plasma irradiation of a N_2/CH_4 = 90/10 gas mixture at 1.6 mbar (MP). The imaginary part of complex reflective indices, *k*, for wavelengths less than 2.7 μm should be treated only as upper limits.

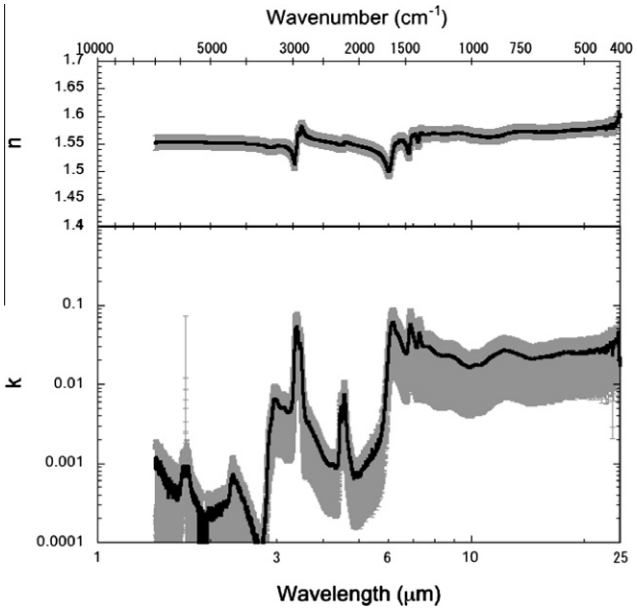

Fig. 7. Optical constants of Titan tholins generated by cold plasma irradiation of a N_2/CH_4 = 90/10 gas mixture at 23 mbar (HP). The rather conservative uncertainty in *k* of approximately 50% comes from the uncertainty of the film thickness. The imaginary part of complex reflective indices, *k*, for wavelengths less than 2.7 μm should be treated only as upper limits.

observations with constrained thickness, as described in Section 4. The uncertainty of *k* demonstrates that the effect of random noise in each transmittance and reflectance spectrum is almost negligible compared to the fitting residuals for different transmittance and reflectance spectra. The uncertainty of *k* is typically less than 10%. For the spectral region where the film is optically thin, it can be as large as 100%. In such optically thin regions, the *k*-values here should be treated only as upper limits. The uncertainties of $n(\lambda)$ are simply estimated from the error propagation of the uncertainty of *n* at 1.547 μm and from the possible range of $n(\lambda)$ determined independently from each sample. As described, the uncertainty of $n(\lambda)$ is generally less than 0.01 at wavelengths shorter than 10 μm, but could increase up to 0.2 at wavelengths longer than 10 μm because of the uncertainty of k(λ) at wavelengths longer than 20 μm.

Finally, there is only one reliable transmittance spectrum for the HP tholin on KBr sample generated at 23 mbar. Because no clear fringe was observed at near-IR wavelengths for the sample deposited on the KBr substrate, the refractive index, *n*, seems very close to that of the KBr substrate. This fact puts more constraint on *n* at 1.547 μm between 1.54 and 1.554. The thickness was estimated from a different sample on a quartz substrate that was generated at the same experiment run. The transmittance measurement (0.185 μm to 3.3 μm) of the sample on quartz clearly shows multiple fringes, and the thickness was determined as 3.4 μm. The absorption band at 3.0 μm in the overlapped region of two sample measurements on KBr and on Qz provides a rough estimate of the thickness of the HP sample on KBr substrate as 2.2 ± 1.2 μm. Fig. 7 shows the optical constants of the HP tholin. The uncertainty is very large, but it would still be useful to constrain the range of *n* and *k* for the HP tholin. We believe the error bars of *k* are better than 50%, but no further constraint can be obtained at this moment.

Table 3 lists a small selection of the determined optical constants, and the complete lists are available electronically as supplements.

6. Discussion

6.1. Comparisons with previous work

There have been only a few studies of optical constants of Titan tholins, or related Titan haze analogues, in the mid-IR wavelengths (2.5–25 μm). Here, we are comparing our results to previously published optical constants in the mid-IR wavelength region.

Khare et al. (1984) conducted a thorough study of optical constants of a Titan tholin at wavelengths from soft X-ray to microwave frequencies. This Titan tholin was generated with a magnetically enhanced DC plasma discharge in an N_2/CH_4 = 90/10 gas mixture at 0.2 mbar. The flow rate was approximately 3 sccm (standard cubic centimeter per minute), which is eight times slower than our condition for the LP tholins (Imanaka et al., 2004). The DC current was 15 mA with a 200 V potential difference (~3 W power). The *k*-values in the mid-IR region were determined from transmittance measurements of a film sample deposited on CsI substrate using a simple Lambert's law. After combining *k*-values measured at all other wavelength regions, the Kramers–Kronig analysis was conducted. The claimed uncertainty of *k* is approximately 30%. This work is still the only in-depth study of optical constants of Titan tholin over such a wide range of wavelength. However, the tabulated spectral resolution is typically larger than 0.3–0.7 μm in the mid-IR wavelengths.

Fig. 8 summarizes the optical constants of three types of Titan tholins in this study with those measured by Khare et al. (1984). It shows that all of our optical constants (both *n* and *k*) are significantly smaller than those of Khare et al. (1984) with our LP sample being closest to the one by Khare et al. (1984). Fig. 9 shows the comparison in the absorption coefficients, α (cm^{-1}) (=$4\pi k/\lambda$), in order to demonstrate detailed absorption features on a linear scale. The detailed assessment of possible functional groups and their systematic variations have already been described in our previous work (Imanaka et al., 2004), and a reader interested in those chemical assignments may refer to such works (Imanaka et al., 2004; Cruikshank et al., 2005; Bernard et al., 2006; Quirico et al., 2008). Here, we briefly mention the quantitative aspects.

Table 3
A small portion of the optical constants of Titan tholins generated from a N_2/CH_4 = 90/10 gas mixture at three different pressures. The complete tabulated optical constants with uncertainties are available electronically as supplements.

Wavelength (μm)	Wavenumber (cm^{-1})	0.26 mbar (LP)		1.6 mbar (MP)		23 mbar (HP)	
		n	*k*	*n*	*k*	*n*	*k*
2.500	4000	1.592	7.81E−04	1.558	6.45E−04	1.551	2.52E−04
2.513	3980	1.592	8.16E−04	1.558	6.18E−04	1.551	2.44E−04
2.525	3960	1.591	8.65E−04	1.558	5.88E−04	1.551	2.11E−04
2.538	3940	1.591	9.14E−04	1.558	5.59E−04	1.551	2.12E−04
2.551	3920	1.591	9.59E−04	1.557	5.36E−04	1.551	1.90E−04
2.564	3900	1.590	1.00E−03	1.557	5.27E−04	1.551	1.82E−04
2.577	3880	1.590	1.05E−03	1.557	5.25E−04	1.550	1.62E−04
2.591	3860	1.590	1.08E−03	1.556	5.37E−04	1.550	1.41E−04
2.604	3840	1.589	1.10E−03	1.556	5.54E−04	1.550	1.48E−04
2.618	3820	1.589	1.11E−03	1.556	5.71E−04	1.550	1.31E−04
2.632	3800	1.588	1.10E−03	1.556	5.89E−04	1.550	1.10E−04
2.646	3780	1.588	1.09E−03	1.555	5.95E−04	1.550	9.80E−05
2.660	3760	1.587	1.07E−03	1.555	5.99E−04	1.550	9.27E−05
2.674	3740	1.587	1.07E−03	1.554	6.13E−04	1.549	1.05E−04
2.688	3720	1.586	9.93E−04	1.554	5.90E−04	1.549	7.47E−05
2.703	3700	1.585	9.43E−04	1.553	5.94E−04	1.549	1.00E−07
2.717	3680	1.584	9.36E−04	1.553	6.86E−04	1.549	1.00E−07
2.732	3660	1.583	1.02E−03	1.552	1.01E−03	1.549	3.14E−05
2.747	3640	1.582	1.19E−03	1.551	1.45E−03	1.548	8.07E−05
2.762	3620	1.581	1.41E−03	1.551	1.93E−03	1.548	1.04E−04
2.778	3600	1.580	1.68E−03	1.550	2.34E−03	1.548	1.27E−04
2.793	3580	1.579	1.99E−03	1.550	2.66E−03	1.547	1.73E−04
2.809	3560	1.577	2.39E−03	1.549	2.88E−03	1.547	2.14E−04
2.825	3540	1.575	3.04E−03	1.548	3.11E−03	1.546	3.52E−04
2.841	3520	1.572	4.57E−03	1.546	3.72E−03	1.546	7.46E−04
2.857	3500	1.569	7.56E−03	1.544	5.47E−03	1.545	1.47E−03
2.874	3480	1.568	1.12E−02	1.544	7.88E−03	1.545	2.22E−03
2.890	3460	1.568	1.45E−02	1.544	9.89E−03	1.545	2.76E−03
2.907	3440	1.568	1.75E−02	1.543	1.15E−02	1.545	3.16E−03
2.924	3420	1.568	2.08E−02	1.543	1.35E−02	1.544	3.85E−03
2.941	3400	1.568	2.49E−02	1.542	1.71E−02	1.544	5.10E−03
2.959	3380	1.570	2.91E−02	1.545	2.16E−02	1.545	6.27E−03
2.976	3360	1.573	3.25E−02	1.549	2.37E−02	1.546	6.53E−03
2.994	3340	1.577	3.49E−02	1.552	2.34E−02	1.546	6.32E−03
3.012	3320	1.582	3.55E−02	1.556	2.26E−02	1.547	6.19E−03
3.030	3300	1.585	3.46E−02	1.557	2.12E−02	1.547	5.86E−03
3.049	3280	1.587	3.32E−02	1.558	1.97E−02	1.547	5.44E−03
3.067	3260	1.588	3.22E−02	1.558	1.87E−02	1.547	5.16E−03
3.086	3240	1.589	3.21E−02	1.558	1.84E−02	1.547	5.05E−03
3.106	3220	1.590	3.26E−02	1.559	1.84E−02	1.546	5.12E−03
3.125	3200	1.592	3.28E−02	1.560	1.84E−02	1.546	5.19E−03
3.145	3180	1.594	3.23E−02	1.561	1.79E−02	1.546	5.16E−03
3.165	3160	1.596	3.11E−02	1.561	1.68E−02	1.546	4.95E−03
3.185	3140	1.597	2.99E−02	1.562	1.57E−02	1.545	4.71E−03
3.205	3120	1.598	2.87E−02	1.561	1.47E−02	1.544	4.50E−03
3.226	3100	1.598	2.76E−02	1.560	1.40E−02	1.543	4.44E−03
3.247	3080	1.598	2.66E−02	1.560	1.36E−02	1.542	4.49E−03
3.268	3060	1.598	2.58E−02	1.559	1.33E−02	1.540	4.56E−03
3.289	3040	1.599	2.50E−02	1.557	1.30E−02	1.537	4.84E−03
3.311	3020	1.598	2.45E−02	1.555	1.32E−02	1.533	5.64E−03
3.333	3000	1.596	2.51E−02	1.551	1.57E−02	1.525	8.98E−03
3.356	2980	1.595	2.84E−02	1.548	2.40E−02	1.516	2.21E−02
3.378	2960	1.600	3.03E−02	1.556	3.20E−02	1.525	4.74E−02
3.401	2940	1.601	3.02E−02	1.562	3.40E−02	1.543	4.98E−02
3.425	2920	1.606	2.93E−02	1.572	3.19E−02	1.564	4.97E−02
3.448	2900	1.607	2.55E−02	1.574	2.47E−02	1.571	3.48E−02
3.472	2880	1.607	2.40E−02	1.574	2.32E−02	1.567	2.95E−02
3.497	2860	1.609	2.23E−02	1.579	2.03E−02	1.578	2.89E−02
3.521	2840	1.609	1.92E−02	1.579	1.44E−02	1.581	1.54E−02
3.546	2820	1.608	1.71E−02	1.577	1.07E−02	1.575	7.43E−03
3.571	2800	1.607	1.57E−02	1.574	8.78E−03	1.570	4.87E−03
3.597	2780	1.606	1.47E−02	1.573	7.67E−03	1.567	3.79E−03
3.623	2760	1.605	1.39E−02	1.571	7.06E−03	1.565	3.35E−03
3.650	2740	1.605	1.32E−02	1.570	6.69E−03	1.563	3.31E−03
3.676	2720	1.604	1.24E−02	1.569	6.25E−03	1.562	3.18E−03
3.704	2700	1.603	1.15E−02	1.569	5.84E−03	1.561	2.83E−03
3.731	2680	1.603	1.07E−02	1.568	5.51E−03	1.561	2.64E−03
3.759	2660	1.602	9.94E−03	1.567	5.22E−03	1.560	2.46E−03
3.788	2640	1.601	9.24E−03	1.567	4.95E−03	1.559	2.28E−03
3.817	2620	1.600	8.62E−03	1.566	4.71E−03	1.559	2.14E−03
3.846	2600	1.599	8.07E−03	1.565	4.42E−03	1.558	1.99E−03
3.876	2580	1.598	7.63E−03	1.565	4.15E−03	1.558	1.82E−03

Table 3 (*continued*)

Wavelength (μm)	Wavenumber (cm^{-1})	0.26 mbar (LP)		1.6 mbar (MP)		23 mbar (HP)	
		n	*k*	*n*	*k*	*n*	*k*
3.906	2560	1.597	7.26E−03	1.564	3.89E−03	1.557	1.65E−03
3.937	2540	1.596	6.97E−03	1.564	3.66E−03	1.557	1.51E−03
3.968	2520	1.595	6.72E−03	1.563	3.43E−03	1.556	1.38E−03
4.000	2500	1.594	6.49E−03	1.562	3.23E−03	1.556	1.26E−03
4.032	2480	1.593	6.32E−03	1.561	3.08E−03	1.555	1.17E−03
4.065	2460	1.592	6.18E−03	1.561	2.96E−03	1.555	1.10E−03
4.098	2440	1.591	6.07E−03	1.560	2.88E−03	1.555	1.04E−03
4.132	2420	1.590	6.00E−03	1.559	2.84E−03	1.554	9.88E−04
4.167	2400	1.589	5.92E−03	1.558	2.82E−03	1.554	9.60E−04
4.202	2380	1.588	5.82E−03	1.557	2.83E−03	1.553	9.46E−04
4.237	2360	1.587	5.73E−03	1.557	2.93E−03	1.553	9.76E−04
4.274	2340	1.585	5.66E−03	1.555	2.95E−03	1.552	9.62E−04
4.310	2320	1.584	5.57E−03	1.554	2.95E−03	1.552	9.12E−04
4.348	2300	1.582	5.47E−03	1.553	3.02E−03	1.551	8.78E−04
4.386	2280	1.580	5.46E−03	1.550	3.35E−03	1.550	9.47E−04
4.425	2260	1.577	6.01E−03	1.545	6.15E−03	1.548	1.59E−03
4.464	2240	1.575	7.69E−03	1.551	1.51E−02	1.549	5.15E−03
4.505	2220	1.571	1.06E−02	1.549	8.49E−03	1.549	3.50E−03
4.545	2200	1.570	1.70E−02	1.544	1.59E−02	1.549	6.12E−03
4.587	2180	1.575	2.28E−02	1.556	2.58E−02	1.553	6.76E−03
4.630	2160	1.581	2.31E−02	1.564	1.59E−02	1.554	3.09E−03
4.673	2140	1.588	1.86E−02	1.562	1.08E−02	1.553	1.74E−03
4.717	2120	1.586	1.09E−02	1.561	8.65E−03	1.552	1.27E−03
4.762	2100	1.583	7.70E−03	1.560	7.76E−03	1.551	1.02E−03
4.808	2080	1.579	5.80E−03	1.560	5.52E−03	1.550	7.75E−04
4.854	2060	1.576	4.64E−03	1.557	3.31E−03	1.549	7.58E−04
4.902	2040	1.573	4.29E−03	1.555	2.68E−03	1.549	7.46E−04
4.950	2020	1.569	4.29E−03	1.553	2.52E−03	1.548	6.69E−04
5.000	2000	1.566	4.40E−03	1.551	2.46E−03	1.547	7.59E−04
5.051	1980	1.563	4.50E−03	1.549	2.43E−03	1.546	7.45E−04
5.102	1960	1.560	4.67E−03	1.548	2.45E−03	1.546	8.39E−04
5.155	1940	1.557	4.81E−03	1.546	2.49E−03	1.545	8.87E−04
5.208	1920	1.553	4.94E−03	1.544	2.54E−03	1.544	9.41E−04
5.263	1900	1.549	5.08E−03	1.542	2.61E−03	1.543	9.99E−04
5.319	1880	1.545	5.26E−03	1.540	2.70E−03	1.542	1.06E−03
5.376	1860	1.540	5.46E−03	1.537	2.79E−03	1.541	1.13E−03
5.435	1840	1.534	5.71E−03	1.535	2.90E−03	1.540	1.21E−03
5.495	1820	1.527	6.09E−03	1.531	3.06E−03	1.538	1.28E−03
5.556	1800	1.518	6.77E−03	1.527	3.32E−03	1.536	1.52E−03
5.618	1780	1.507	8.04E−03	1.523	3.64E−03	1.534	1.66E−03
5.682	1760	1.493	1.10E−02	1.517	4.24E−03	1.532	1.87E−03
5.747	1740	1.475	1.76E−02	1.508	5.72E−03	1.528	2.57E−03
5.814	1720	1.453	3.11E−02	1.496	8.93E−03	1.523	3.45E−03
5.882	1700	1.429	5.80E−02	1.479	1.95E−02	1.516	7.31E−03
5.952	1680	1.412	9.98E−02	1.460	4.32E−02	1.506	1.52E−02
6.024	1660	1.419	1.61E−01	1.460	9.51E−02	1.502	3.64E−02
6.098	1640	1.460	2.07E−01	1.507	1.25E−01	1.517	5.56E−02
6.173	1620	1.510	2.20E−01	1.543	1.21E−01	1.537	6.00E−02
6.250	1600	1.542	2.09E−01	1.565	1.02E−01	1.550	4.88E−02
6.329	1580	1.560	2.13E−01	1.571	8.93E−02	1.553	4.33E−02
6.410	1560	1.588	2.16E−01	1.578	8.25E−02	1.556	3.98E−02
6.494	1540	1.614	2.05E−01	1.582	6.90E−02	1.558	3.35E−02
6.579	1520	1.636	1.85E−01	1.579	5.89E−02	1.555	2.74E−02
6.667	1500	1.647	1.62E−01	1.577	5.21E−02	1.550	2.47E−02
6.757	1480	1.641	1.44E−01	1.565	4.83E−02	1.537	2.85E−02
6.849	1460	1.632	1.46E−01	1.561	6.56E−02	1.544	5.61E−02
6.944	1440	1.641	1.49E−01	1.573	6.50E−02	1.566	4.60E−02
7.042	1420	1.651	1.43E−01	1.580	6.67E−02	1.567	3.64E−02
7.143	1400	1.657	1.32E−01	1.581	5.30E−02	1.561	2.91E−02
7.246	1380	1.657	1.31E−01	1.579	5.98E−02	1.559	4.45E−02
7.353	1360	1.662	1.22E−01	1.582	5.30E−02	1.571	3.29E−02
7.463	1340	1.662	1.19E−01	1.581	5.34E−02	1.567	3.02E−02
7.576	1320	1.667	1.13E−01	1.583	5.29E−02	1.567	3.03E−02
7.692	1300	1.670	1.08E−01	1.585	5.14E−02	1.569	2.98E−02
7.813	1280	1.670	1.02E−01	1.586	4.86E−02	1.569	2.82E−02
7.937	1260	1.670	9.75E−02	1.586	4.56E−02	1.570	2.61E−02
8.065	1240	1.670	9.30E−02	1.584	4.36E−02	1.569	2.44E−02
8.197	1220	1.672	8.84E−02	1.584	4.25E−02	1.569	2.36E−02
8.333	1200	1.671	8.37E−02	1.582	4.21E−02	1.568	2.31E−02
8.475	1180	1.669	8.09E−02	1.580	4.32E−02	1.568	2.31E−02
8.621	1160	1.667	7.94E−02	1.581	4.51E−02	1.568	2.32E−02
8.772	1140	1.668	7.75E−02	1.583	4.61E−02	1.569	2.30E−02
8.929	1120	1.669	7.53E−02	1.586	4.55E−02	1.570	2.23E−02

(*continued on next page*)

Table 3 (*continued*)

Wavelength (μm)	Wavenumber (cm^{-1})	0.26 mbar (LP)		1.6 mbar (MP)		23 mbar (HP)	
		n	*k*	*n*	*k*	*n*	*k*
9.091	1100	1.670	7.20E−02	1.587	4.30E−02	1.570	2.12E−02
9.259	1080	1.670	6.73E−02	1.587	4.02E−02	1.570	1.98E−02
9.434	1060	1.668	6.25E−02	1.586	3.75E−02	1.570	1.83E−02
9.615	1040	1.666	5.95E−02	1.585	3.59E−02	1.569	1.74E−02
9.804	1020	1.663	5.54E−02	1.582	3.47E−02	1.568	1.66E−02
10.000	1000	1.656	5.52E−02	1.578	3.52E−02	1.566	1.67E−02
10.204	980	1.656	5.80E−02	1.576	3.68E−02	1.565	1.77E−02
10.417	960	1.654	5.43E−02	1.573	3.84E−02	1.565	1.75E−02
10.638	940	1.651	5.35E−02	1.572	4.20E−02	1.564	1.78E−02
10.870	920	1.647	5.39E−02	1.572	4.63E−02	1.563	1.91E−02
11.111	900	1.643	5.44E−02	1.573	5.00E−02	1.563	2.07E−02
11.364	880	1.639	5.64E−02	1.574	5.34E−02	1.563	2.26E−02
11.628	860	1.635	6.00E−02	1.578	5.58E−02	1.564	2.40E−02
11.905	840	1.630	6.70E−02	1.581	5.72E−02	1.565	2.53E−02
12.195	820	1.633	7.78E−02	1.584	5.83E−02	1.567	2.69E−02
12.500	800	1.637	7.88E−02	1.587	5.73E−02	1.569	2.65E−02
12.821	780	1.639	8.13E−02	1.588	5.61E−02	1.571	2.59E−02
13.158	760	1.643	8.41E−02	1.590	5.59E−02	1.573	2.46E−02
13.514	740	1.646	8.59E−02	1.591	5.57E−02	1.573	2.37E−02
13.889	720	1.648	8.65E−02	1.592	5.50E−02	1.574	2.24E−02
14.286	700	1.648	8.74E−02	1.591	5.48E−02	1.573	2.13E−02
14.706	680	1.650	8.97E−02	1.591	5.59E−02	1.572	2.09E−02
15.152	660	1.652	9.40E−02	1.592	5.77E−02	1.572	2.18E−02
15.625	640	1.655	9.74E−02	1.593	5.94E−02	1.572	2.21E−02
16.129	620	1.660	1.01E−01	1.595	6.09E−02	1.572	2.25E−02
16.667	600	1.665	1.03E−01	1.597	6.24E−02	1.572	2.36E−02
17.241	580	1.673	1.04E−01	1.600	6.45E−02	1.573	2.47E−02
17.857	560	1.679	1.04E−01	1.604	6.54E−02	1.574	2.53E−02
18.519	540	1.686	1.00E−01	1.607	6.34E−02	1.575	2.49E−02
19.231	520	1.688	9.55E−02	1.608	6.22E−02	1.576	2.48E−02
20.000	500	1.691	9.15E−02	1.611	6.09E−02	1.577	2.49E−02
20.833	480	1.695	9.04E−02	1.611	6.15E−02	1.579	2.57E−02
21.739	460	1.690	8.16E−02	1.612	6.15E−02	1.580	2.75E−02
22.727	440	1.684	8.12E−02	1.612	6.21E−02	1.580	2.52E−02
23.810	420	1.672	8.67E−02	1.613	6.62E−02	1.585	2.68E−02
25.000	400	1.717	1.01E−01	1.641	6.51E−02	1.604	1.64E−02

(1) The $k(\lambda)$ of our LP tholin shows very similar values to those of Khare et al. (1984) at 2200–2100 cm^{-1} (4.6 μm) (CN nitrile bands) and at 1600 cm^{-1} (6.25 μm) broad absorption band. However, the $k(\lambda)$ around 3 μm and 10–25 μm is approximately 50% of those of Khare et al. (1984). The difference of the plasma chamber apparatus, the difference of flow rate, and possible contamination could be the reason for such difference in corresponding $k(\lambda)$. As described later, such differences in $k(\lambda)$ are potentially important for interpretation of observations of Titan by the Voyager and the Cassini.

(2) The increase in strength of absorption bands around 1600 cm^{-1} (6.25 μm) is evident if the deposition pressure is decreased. The possible origins of these bands are the functional groups of C=C, C=N, and $-NH_2$ (Imanaka et al., 2004). The increase of unsaturated bonds (C=C, or C=N) in the mid-IR wavelengths may correlate with the increase of absorption strengths in the UV/Vis wavelengths (Imanaka et al., 2004; Cruikshank et al., 2005). Even though only a few quantitative IR absorbance studies of nitrogenated amorphous hydrocarbon (a-CHN) materials exist, the range of our absorption coefficient (α; 2000–5000 cm^{-1}) near 1600 cm^{-1} (6.25 μm) is generally consistent with the previous works (Fanchini et al., 2002, 2003; Lazar et al., 2003, 2005; Bouchet-Fabre et al., 2004, 2005).

(3) The relative ratio of 3.4 μm bands (C–H stretching bands) and 3 μm bands (N–H stretching/or/O–H stretching bands) was found to increase if the deposition pressure increased (Imanaka et al., 2004). This HP tholin contains less nitrogen and more hydrogen than the LP tholin (Imanaka et al., 2004), and this is confirmed by recent ultra-high-resolution mass spectrometric analysis (Imanaka and Smith, 2010). The largest 3.4 μm absorption peak is approximately 2000 (±1000) cm^{-1} for the HP tholin. This is roughly the same order as the 3.4 μm absorption intensity for "polymer-like hydrogenated carbons" (H/C ∼ 1.5–1.7) (De Martino et al., 1995; Ristein et al., 1998) and "hydrogenated amorphous carbons" with high hydrogen contents (H/C ∼ 0.5–1) (Dischler and Bayer, 1990; Tanaka et al., 1990; Dekempeneer et al., 1992; Furton et al., 1999; Mennella et al., 2002). It should be noticed that the C–H band strength in the 3.4 μm region of amorphous hydrogenated carbons varied by an order of magnitude (Silva, 2003). However, the absolute intensity overlaps with our three types of tholins, thereby the range of our optical constants at 3.4 μm bands seems reasonable for complex organic materials.

Tran et al. (2003) generated photochemical organic polymers by 185 nm/254 nm UV light irradiation of gas mixtures of C_2H_2, C_2H_4, HC_3N diluted with N_2/CH_4. The 50–100 nm polymer film was scraped from the collection plate and was simply accumulated on NaCl disk for transmittance measurement in 2.5–16 μm wavelengths. They provide a rough estimation of k from Lambert's law, and the k at the 3.4 μm bands is shown to be approximately 0.2 ($\alpha \sim 7000$ cm^{-1}). However, their procedure may result in large uncertainties because of their thickness estimation and their arbitrary background correction (Fig. 7 in Tran et al. (2003)). Since there are no tabulated data in the mid-IR wavelengths, we simply mention that their photochemical aerosol analogues show similar relative absorbance to our HP tholin sample.

Finally, we comment on the uncertainty of the absorption feature at 750 cm^{-1} (13.3 μm) for the LP tholins. Imanaka et al.

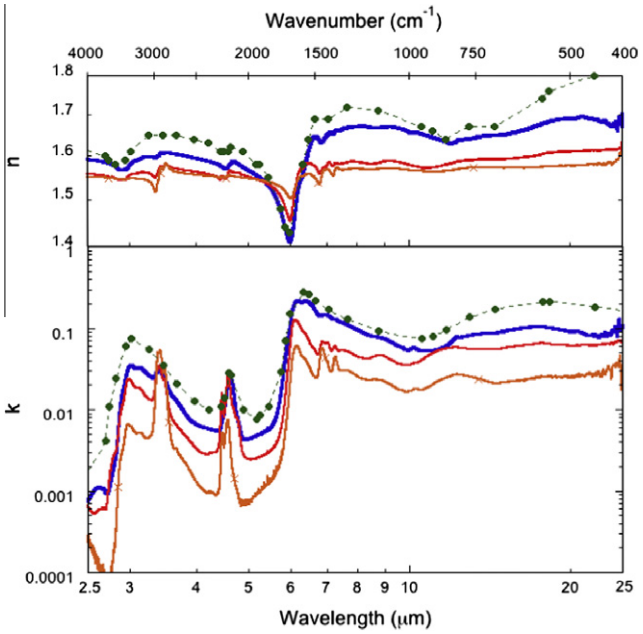

Fig. 8. Summary of optical constants of three types of Titan tholins in this study. Optical constants of the Titan tholins generated at 0.26 mbar (blue line), those at 1.6 mbar (red line), and those at 23 mbar (orange line). All the data of the optical constants of Titan tholin (Khare et al., 1984) in the corresponding wavelength region are shown as green dots. (For interpretation of the references to color in this figure legend, the reader is referred to the web version of this article.)

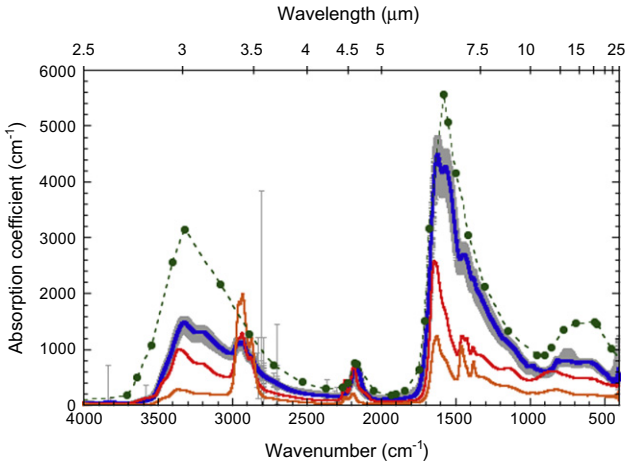

Fig. 9. Absorption coefficients, $\alpha = 4\pi k/\lambda$ (cm^{-1}), of Titan tholins generated at 0.26 mbar (blue line), those at 1.6 mbar (red line), and those at 23 mbar (orange line). All the data points from the optical constants of Titan tholin (Khare et al., 1984) in the corresponding wavelength region are shown as green dots. For clarity, only the uncertainty for the Titan tholin at 0.26 mbar is shown in gray. (For interpretation of the references to color in this figure legend, the reader is referred to the web version of this article.)

(2004) observed an absorption feature at 750 cm^{-1}, and they tentatively assigned it to possible aromatic C–H bands. However, this absorption feature was not repeatedly observed. The observed feature could be caused by contaminations, but the exact reason is not known at this moment.

6.2. Implication for Titan

Titan's high altitude haze probably consists of complex organic materials (McKay et al., 2001; Waite et al., 2009). The Voyager and ground-based observations were interpreted by assuming optical properties of haze particles with slight modifications of the optical constants of the Khare et al. (1984) Titan tholin (see review by McKay et al. (2001)). The Cassini–Huygens observations put tighter constraints on Titan's haze optical properties and its morphology (Tomasko and West, 2009; Lavvas et al., 2010). Recently, the VIMS and the CIRS observations of Titan's limb profiles in the mid-IR wavelengths have just revealed deeper insight into the chemical properties of Titan's haze (Bellucci et al., 2009; Rannou et al., 2010; Vinatier et al., 2010; Anderson and Samuelson, 2011). In this section, we briefly discuss the implication of our new optical constants of three types of Titan tholins in the mid-IR wavelengths.

6.2.1. New constraints from the Cassini VIMS observations of Titan's haze

The solar occultation observation by the Cassini VIMS through the atmosphere of Titan indicates a large opacity source at 3.4 μm below 480 km altitude that cannot be simply explained by gaseous CH_4 absorption (Bellucci et al., 2009). They attributed this additional source of extinction to haze particles as the implication of complex organic materials rich in C–H bonds. They demonstrated that the haze optical properties are inconsistent at 3 μm if the optical constants of the Khare et al. (1984) Titan tholin were assumed for the building material of Titan's haze. Rannou et al. (2010) further studied the possible optical properties of Titan haze in wavelength region between 0.3 and 4 μm from multiple observations by the DISR and the VIMS. They constrained the required k-values at wavelengths of 2.76–2.98 μm from the VIMS high-phase-angle spectral images. They also retrieved the $k(\lambda)$ of haze particles between 3 and 4 μm with a prominent peak at 3.4 μm and a possible secondary minor peak at 3 μm. The k(3.4 μm) is required to be 0.6 in their model if haze particles are solely responsible for the observed absorption feature.

Fig. 10 compares the retrieved imaginary part of complex refractive indices (k) from the VIMS observation (Rannou et al., 2010) with the k-values of laboratory synthesized Titan tholins. It is obvious that none of the Titan tholins in this study nor the Titan tholin by Khare et al. (1984) can explain such a large retrieved k at 3.4 μm. Even the largest k(3.4 μm) ~0.06 ± 0.03 of the HP tholin is 7–10 times smaller than the retrieved k. If all the assumptions in the haze model (Rannou et al., 2010) are correct, this observed absorption at 3.4 μm cannot be explained by haze particles consisting of any of the Titan tholins in this study.

A temperature dependence of optical constants of tholin could be the reason for this discrepancy. However, this is unlikely because the bidirectional reflectance spectrum of a Titan tholin covering 7000–400 cm^{-1} only shows slight temperature dependence (Brucato et al., 2010). As described in Section 6.1, most of the complex carbonaceous materials, within our limited knowledge, may not account for such a large k at 3.4 μm. It is interesting to note that the peak intensity of $k(\lambda)$ at 3.4 μm bands of the HP tholin is of a similar order as those of the amorphous phase of simple nitriles condensates, such as CH_3CN and C_2H_5CN (Moore et al., 2010). Crystalline condensates of very large saturated hydrocarbons/nitriles, such as those molecules much larger than n-heptane (k(3.4 μm) = 0.137) and n-decane (k(3.4 μm) = 0.225), (Tuntomo et al., 1992) or simple hydrocarbon polymers, such as poly-ethylene (k(3.4 μm) = 0.35, (Zolotarev et al., 2006)) could be the candidates for such materials showing a large value of k at 3.4 μm. However, those absorption peaks are very narrow, and no single components may explain the broad absorption feature observed at 3.4 μm.

The above discrepancy could be caused by the assumptions in the haze model by Rannou et al. (2010). They assumed that the haze particles consist of a single component, whose optical constants at 3.6–3.8 μm are those of the Titan tholin by Khare et al. (1984). However, the slope of the $k(\lambda)$ value at 3.6–3.8 μm is most

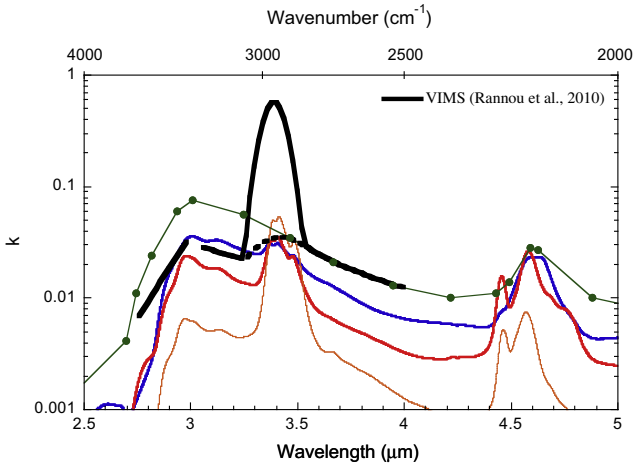

Fig. 10. Comparison with the recently derived imaginary part of refractive indices of Titan's haze from the Cassini VIMS observations (Rannou et al., 2010). The black dashed line between 3.2 and 3.4 μm (*k_smallest*) corresponds to an assumption that the observed opacity at 3.4 μm caused by sources other than Titan's haze. The *k*-values of the Titan tholins generated at 0.26 mbar (blue line), those at 1.6 mbar (red line), and those at 23 mbar (orange line) are shown. All the *k*-values of Titan tholin (Khare et al., 1984) in the corresponding wavelength region are shown as green dots. (For interpretation of the references to color in this figure legend, the reader is referred to the web version of this article.)

likely the tailing off of the large bands at 3 μm region (Imanaka et al., 2004). Thus, it is unlikely that the $k(\lambda)$ value shows such a discontinuity from 3 μm to 3.8 μm as appeared in the retrieved *k* by Rannou et al. (2010) (Fig. 10). As mentioned by Rannou et al. (2010), the attempt to scale $k(\lambda)$ at 3.6–3.8 μm to 0.1 times those of Khare et al. (1984) only decreased the retrieved *k* at 3.4 μm to 0.43. This scaling might be reasonable since the relative strength of 3.4 μm band and 3 μm band for the HP tholin agrees well. Such agreement may imply a significant amount of nitrogen inclusion in the haze particles, but the maximum nitrogen content is unknown. However, this HP tholin alone cannot explain such a large absorption at 3.4 μm.

Another possibility is the uncertainty of the absolute haze number density profile in Titan's atmosphere. Rannou et al. (2010) and Bellucci et al. (2009) estimated the haze number density profiles to meet the required haze opacity constrained by the DISR or VIMS observations with assumption of haze particles whose optical properties are similar to those of the Titan tholin by Khare et al. (1984) at wavelengths up to 0.8 μm. If Titan haze material has much lower *k* in visible wavelengths, such as our MP/HP tholins (Imanaka et al., 2004, 2005), the derived haze number density could be underestimated, and such an underestimation of haze particles could cause overestimation of *k* in 3.4 μm. Furthermore, it is unlikely that Titan haze materials consist of a single homogeneous component. It might be a mixture of complex organic materials/condensates from different origins in the different altitudes. For such a case, a simple assumption of optical constants represented just as a single Titan tholin may not be valid. Further studies of haze modeling and additional laboratory work are desired in the future.

6.2.2. The spectral features retrieved from the CIRS

The thermal infrared emissions of Titan measured by the Voyager IRIS and the Cassini CIRS are also able to put constraints on the haze properties in the stratosphere of Titan. The haze optical thickness shows monotonic increase from 250 cm^{-1} to 600 cm^{-1}, which was consistent with models using the optical constants of the Khare et al. (1984) Titan tholin (Samuelson and Mayo, 1991; Mayo and Samuelson, 2005). This continuous emission feature is also observed by the Cassini CIRS (de Kok et al., 2007; Anderson and Samuelson, 2011), and is attributed to a uniform haze component in the stratosphere. Anderson and Samuelson (2011) also observed a very broad emission peak at 140 cm^{-1} whose spectral shape does not change at altitudes below 300 km. They mentioned that such an emission peak is absent in the derived *k*-values of the Khare et al. (1984) Titan tholin. Simultaneous analysis of the geometric albedo in the visible wavelengths and the thermal infrared emission demonstrated the optical properties of Titan's haze in the thermal infrared (200–600 cm^{-1}) had to be reduced from those of Khare et al. (1984) by factor of 0.5 (Toon et al., 1988; McKay et al., 1989) and of 0.3–0.8 (Courtin et al., 1995). Our new optical constants are 2–10 times lower than that of Khare et al. (1984) at 500 cm^{-1}, and might satisfy such requirements.

We limit further discussion to the mid-IR wavelengths where our measurement spectral range overlaps. Interesting spectral features have been obtained from the analysis of continuum emission of limb spectra in the 600–1420 cm^{-1} region by the Cassini CIRS (Vinatier et al., 2010), where only limited information was extracted from the analysis of the Voyager IRIS data (Coustenis and Bezard, 1995). They retrieved the haze extinction profiles at the 3–0.02 mbar range (altitudes of ~150–350 km). Three main spectral features are observed at 630 cm^{-1}, 745 cm^{-1}, and 1390 cm^{-1} with a wide tail extending to ~1000 cm^{-1}. Fig. 11 shows the mean aerosol optical depth at the 0.5 mbar level by Vinatier et al. (2010) with the absorption coefficients, α (cm^{-1}), of Titan tholins determined in this study and by Khare et al. (1984). This comparison is valid in the small particle limit where scattering is negligible (Samuelson and Mayo, 1991). As mentioned by Vinatier et al. (2010), the observed wide tail from 1390 to 1000 cm^{-1} generally agrees with all the tholins. A local peak at 750 cm^{-1} could be attributed to the peak observed in Imanaka et al. (2004), whose uncertainty was already described. There is no local peak at 630 cm^{-1} in the Titan tholins shown here. Such an observed local peak could be attributed to condensates of nitriles or their mixtures (Moore et al., 2010). Vinatier et al. (2010) mentioned that the discrepancy in optical depth from 600 to 750 cm^{-1} with those of Khare et al. (1984). The observed optical depth increases by a factor of 3 from 600 to 750 cm^{-1}, where the absorption coefficient of Khare et al. (1984) is rather flat. Our MP and HP tholins shows a slight increase of absorption coefficient by a factor of 1.5 from 600

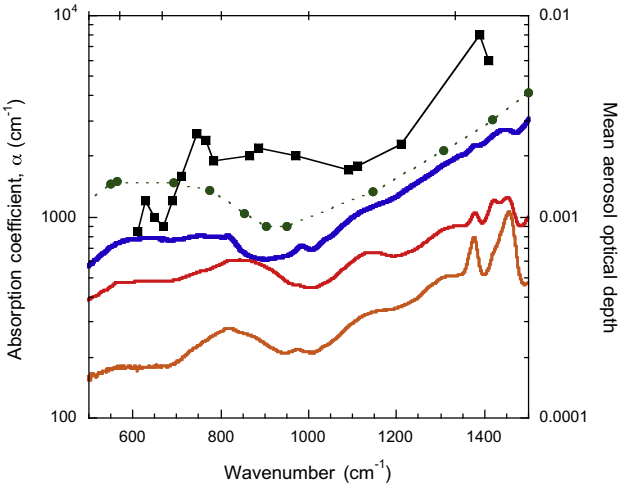

Fig. 11. Comparison of the absorption coefficients of Titan tholins with the mean aerosol optical depth derived from the Cassini CIRS observations (Vinatier et al., 2010). Absorption coefficients, $\alpha = 4\pi k/\lambda$ (cm^{-1}), of Titan tholins generated at 0.26 mbar (blue line), those at 1.6 mbar (red line), and those at 23 mbar (orange line) are shown. All the data points from the optical constants of Titan tholin (Khare et al., 1984) in the corresponding wavelength region are shown as green dots. (For interpretation of the references to color in this figure legend, the reader is referred to the web version of this article.)

to 800 cm^{-1}. Those materials could partially be responsible for such extinction there. The observed optical depth can also interpreted as the broad absorption feature between 700 and 1100 cm^{-1}, although the broad absorption feature observed in the MP and HP tholins ranges only between 700 and 950 cm^{-1}. The possible local peak observed at around 1390 cm^{-1} might correspond to the C–H bending vibration mode, which is clearly observed in our MP and HP tholins (Imanaka et al., 2004). The presence of the C–H bending vibration is consistent with the observed C–H stretching bands at 3.4 μm (Bellucci et al., 2009; Rannou et al., 2010). Because those absorption intensities at 3.4 μm and 7.2 μm are well correlated (Heitz et al., 1998; Ristein et al., 1998), further study is of great interest to fit simultaneously the observed extinction features of both the C–H stretching and bending modes using the optical constants provided in this study.

7. Conclusions

The optical constants of Titan tholins generated by cold plasma irradiation from a N_2/CH_4 gas mixture at three different pressures are provided in the mid-IR wavelength region (2.5–25 μm) with all the uncertainties explicitly shown. The reliable optical constants in the mid-IR wavelength region are potentially useful to give insight to the chemical functional groups found in remote sensing observations now and in the future. In particular, the recent Cassini VIMS and CIRS observations provide new constraints on Titan's haze properties in the wavelength regions covered in this study. Our new optical constants of three types of Titan tholins suggest that no single material fulfills all the observational constraints of the Titan haze materials currently available. Both the VIMS and CIRS observations in the mid-IR wavelengths seem to support the view that Titan's haze particles are composed of hydrogen-rich carbonaceous material at those altitudes. Whether such hydrogen-rich Titan haze materials could explain the observed strong absorption in visible wavelengths is unknown. Because of the similarity between the VIMS observation of relative absorption intensities at the 3 μm and 3.4 μm bands and the HP tholin (C/N ~ 3), a significant amount of nitrogen incorporation in haze materials cannot be fully excluded. The maximum nitrogen contents in Titan's haze particles is not well constrained at this moment. Further detailed investigation of relationships among the formation chemistry, chemical structures, and resulting optical properties of laboratory haze analogs in the future should give a better and more consistent picture of Titan's haze materials.

Acknowledgments

H.I. acknowledges John H. Jackson at Metricon Inc. for the opportunity to analyze our samples with the prism coupler. We also thank anonymous referees for helpful comments that led to the improvement of this manuscript. H.I. acknowledges funding supports from the NASA Cassini Data Analysis Program, NNX10AF08G, and from the NASA Exobiology Program, NNX09AM95G. D.P.C. was supported in part by the Cassini Project.

Appendix A

Formulae used for calculation of the synthetic transmittance and reflectance spectra (T_{cal} and R_{cal}) of a film-substrate system are given. We assume that the film is homogeneous and plane parallel. The coherent multiple reflections inside film (2) between air (1) and a substrate (3) are taken into account. The finite-thickness substrate is much thicker than the wavelength, so that multiple reflections in the substrate are considered as incoherent. We follow the notation by Stenzel et al. (1991).

$$T_{cal} = \frac{|\hat{t}_{123}|^2|\hat{t}_{31}|^2\exp[-2\mathrm{Im}(\hat{\beta}_s)]}{1-|\hat{r}_{321}|^2|\hat{r}_{31}|^2\exp[-4\mathrm{Im}(\hat{\beta}_s)]} \tag{A1}$$

$$R_{cal} = |\hat{r}_{123}|^2 + \frac{|\hat{t}_{123}|^2|\hat{r}_{31}|^2|\hat{t}_{321}|^2\exp[-4\mathrm{Im}(\hat{\beta}_s)]}{1-|\hat{r}_{321}|^2|\hat{r}_{31}|^2\exp[-4\mathrm{Im}(\hat{\beta}_s)]} \tag{A2}$$

Here, $\hat{r}_{abc}$ and $\hat{t}_{abc}$ are the complex amplitude reflection and transmission coefficients for the layers b between the media a and c.

$$\hat{t}_{abc} = \frac{\hat{t}_{ab}\hat{t}_{bc}\exp[i\hat{\beta}]}{1+\hat{r}_{ab}\hat{r}_{bc}\exp[2i\hat{\beta}]} \tag{A3}$$

$$\hat{r}_{abc} = \frac{\hat{r}_{ab}+\hat{r}_{bc}\exp[2i\hat{\beta}]}{1+\hat{r}_{ab}\hat{r}_{bc}\exp[2i\hat{\beta}]} \tag{A4}$$

$$\hat{\beta} = \frac{2\pi d}{\lambda}\sqrt{\hat{n}-sin^2\theta} \tag{A5}$$

θ is the angle of incidence, and $\hat{n}$ is the complex refractive index $(n+ik)$. $\hat{t}_{ab}$ and $\hat{r}_{ab}$ are the complex Fresnel coefficients.

The dependence of optical constants on uncertainties of transmittance and reflectance spectra and thickness are given by the following (del Pozo and Díaz, 1992). The uncertainties of n from T, R, and d ($\sigma_{n,T}, \sigma_{n,R}, \sigma_{n,d}$) can be estimated, and the total uncertainty of n, σ_n, are given as the geometric mean of all uncertainties. Notice that the singularity occurs where the denominator of the following equations becomes zero (del Pozo and Díaz, 1992).

$$\sigma_{n,T}^2 = \frac{\left(\frac{\partial R}{\partial k}\right)^2}{\left[\left(\frac{\partial T}{\partial n}\right)\left(\frac{\partial R}{\partial k}\right)-\left(\frac{\partial T}{\partial k}\right)\left(\frac{\partial R}{\partial n}\right)\right]^2}\sigma_T^2, \tag{A6}$$

$$\sigma_{n,R}^2 = \frac{\left(\frac{\partial T}{\partial k}\right)^2}{\left[\left(\frac{\partial T}{\partial n}\right)\left(\frac{\partial R}{\partial k}\right)-\left(\frac{\partial T}{\partial k}\right)\left(\frac{\partial R}{\partial n}\right)\right]^2}\sigma_R^2, \tag{A7}$$

$$\sigma_{n,d}^2 = \frac{\left[\left(\frac{\partial T}{\partial k}\right)\left(\frac{\partial R}{\partial d}\right)-\left(\frac{\partial T}{\partial d}\right)\left(\frac{\partial R}{\partial k}\right)\right]^2}{\left[\left(\frac{\partial T}{\partial n}\right)\left(\frac{\partial R}{\partial k}\right)-\left(\frac{\partial T}{\partial k}\right)\left(\frac{\partial R}{\partial n}\right)\right]^2}\sigma_d^2, \tag{A8}$$

$$\sigma_n^2 = \sigma_{n,T}^2 + \sigma_{n,R}^2 + \sigma_{n,d}^2. \tag{A9}$$

Similarly, the uncertainty of k, σ_k, can be estimated as follows:

$$\sigma_{k,T}^2 = \frac{\left(\frac{\partial R}{\partial n}\right)^2}{\left[\left(\frac{\partial T}{\partial n}\right)\left(\frac{\partial R}{\partial k}\right)-\left(\frac{\partial T}{\partial k}\right)\left(\frac{\partial R}{\partial n}\right)\right]^2}\sigma_T^2, \tag{A10}$$

$$\sigma_{k,R}^2 = \frac{\left(\frac{\partial T}{\partial n}\right)^2}{\left[\left(\frac{\partial T}{\partial n}\right)\left(\frac{\partial R}{\partial k}\right)-\left(\frac{\partial T}{\partial k}\right)\left(\frac{\partial R}{\partial n}\right)\right]^2}\sigma_R^2, \tag{A11}$$

$$\sigma_{k,d}^2 = \frac{\left[\left(\frac{\partial T}{\partial d}\right)\left(\frac{\partial R}{\partial n}\right)-\left(\frac{\partial T}{\partial n}\right)\left(\frac{\partial R}{\partial d}\right)\right]^2}{\left[\left(\frac{\partial T}{\partial n}\right)\left(\frac{\partial R}{\partial k}\right)-\left(\frac{\partial T}{\partial k}\right)\left(\frac{\partial R}{\partial n}\right)\right]^2}\sigma_d^2, \tag{A12}$$

$$\sigma_k^2 = \sigma_{k,T}^2 + \sigma_{k,R}^2 + \sigma_{k,d}^2. \tag{A13}$$

Appendix B. Supplementary material

Supplementary data associated with this article can be found, in the online version, at doi:10.1016/j.icarus.2011.11.018.

References

Adams, A.C., Schinke, D.P., Capio, C.D., 1979. An evaluation of the prism coupler for measuring the thickness and refractive index of dielectric films on silicon substrates. J. Electrochem. Soc. 126, 1539–1543.

Ahrenkiel, R.K., 1971. Modified Kramers–Kronig analysis of optical spectra. J. Opt. Soc. Am. 61, 1651–1655.

Anderson, C.M., Samuelson, R.E., 2011. Titan's aerosol and stratospheric ice opacities between 18 and 500 μm: Vertical and spectral characteristics from Cassini CIRS. Icarus 212, 762–778.

Beckmann, P., Spizzichino, A., 1963. The Scattering of Electromagnetic Waves from Rough Surfaces. Macmillan, New York.

Bellucci, A., Sicardy, B., Drossart, P., Rannou, P., Nicholson, P.D., Hedman, M., Baines, K.H., Burrati, B., 2009. Titan solar occultation observed by Cassini/VIMS: Gas absorption and constraints on aerosol composition. Icarus 201, 198–216.

Bernard, J.M., Quirico, E., Brissaud, O., Montagnac, G., Reynard, B., McMillan, P., Coll, P., Nguyen, M.J., Raulin, F., Schmitt, B., 2006. Reflectance spectra and chemical structure of Titan's tholins: Application to the analysis of Cassini–Huygens observations. Icarus 185, 301–307.

Born, M., Wolf, E., 1997. Principles of Optics, sixth ed. Cambridge University Press, New York.

Bouchet-Fabre, B., Godet, C., Lacerda, M., Charvet, S., Zellama, K., Ballutaud, D., 2004. Stoichiometry and infrared absorption of amorphous a-$C_{1-x}N_x$:H carbon nitride films. J. Appl. Phys. 95, 3427–3436.

Bouchet-Fabre, B. et al., 2005. Spectroscopic study using FTIR, Raman, XPS and NEXAFS of carbon nitride thin films deposited by RF magnetron sputtering. Thin Solid Films 482, 167–171.

Brucato, J.R., Migliorini, A., Barucci, M.A., Carvano, J.M., Dotto, E., Mennella, V., 2010. Reflectance spectra of Titan tholin between 7000 and 10 cm^{-1} interpretation of Cassini/CIRS observation of Saturn's satellite Phoebe. Astron. Astrophys. 516, A92. doi:10.1051/0004-6361/200912054.

Courtin, R., Gautier, D., McKay, C.P., 1995. Titan's thermal emission spectrum: Reanalysis of the Voyager infrared measurements. Icarus 114, 144–162.

Coustenis, A., Bezard, B., 1995. Titan's atmosphere from Voyager infrared observations: IV. Latitudinal variations of temperature and composition. Icarus 115, 126–140.

Cruikshank, D.P., Imanaka, H., Dalle Ore, C.M., 2005. Tholins as coloring agents on outer Solar System bodies. Adv. Space Res. 36, 178–183.

de Kok, R., Irwin, P.G.J., Teanby, N.A., Nixon, C.A., Jennings, D.E., Fletcher, L., Howett, C., Calcutt, S.B., Bowles, N.E., Flasar, F.M., Taylor, F.W., 2007. Characteristics of Titan's stratospheric aerosols and condensate clouds from Cassini CIRS far-infrared spectra. Icarus 191, 223–235.

De Martino, C., Demichelis, F., Tagliaferro, A., 1995. Determination of the sp^3/sp^2 ratio in a-C:H films by infrared spectrometry analysis. Diamond Rel. Mater. 4, 1210–1215.

Dekempeneer, E.H.A. et al., 1992. R.F. plasma-assisted chemical vapour deposition of diamond-like carbon: Physical and mechanical properties. Thin Solid Films 217, 56–61.

del Pozo, J.M., Díaz, L., 1992. Method for the determination of optical constants of thin films: Dependence on experimental uncertainties. Appl. Opt. 31, 4474–4481.

Dischler, B., Bayer, E., 1990. Properties of amorphous hydrogenated carbon films from ArF laser-induced C_2H_2 photolysis. J. Appl. Phys. 68, 1237–1241.

Fanchini, G.T., Messina, A., Santangelo, G., Paoletti, S., Tucciarone, A., 2002. Vibrational properties and microstructure of reactively sputtered hydrogenated carbon nitrides. J. Appl. Phys. 91, 1155–1165.

Fanchini, G., Tagliaferro, A., Ray, S.C., 2003. Electronic and vibrational structures of amorphous carbon nitrides. Diamond Rel. Mater. 12, 208–218.

Ferrari, A.C. et al., 2000. Density, sp^3 fraction, and cross-sectional structure of amorphous carbon films determined by X-ray reflectivity and electron energy-loss spectroscopy. Phys. Rev. B 62, 11089–11103.

Furton, D.G., Laiho, J.W., Witt, A.N., 1999. The amount of interstellar carbon locked in solid hydrogenated amorphous carbon. Astrophys. J. 526, 752–763.

Gautier, T., Carrasco, N., Buch, A., Szopa, C., Sciamma-O'Brien, E., Cernogora, G., 2011. Nitrile gas chemistry in Titan's atmosphere. Icarus 213, 625–635.

Harbecke, B., 1986. Coherent and incoherent reflection and transmission of multilayer structures. Appl. Phys. B: Lasers Opt. 39, 165–170.

Hasenkopf, C.A., Beaver, M.R., Trainer, M.G., Langley Dewitt, H., Freedman, M.A., Toon, O.B., McKay, C.P., Tolbert, M.A., 2010. Optical properties of Titan and early Earth haze laboratory analogs in the mid-visible. Icarus 207, 903–913.

Hawranek, J.P., Neelakantan, P., Young, R.P., Jones, R.N., 1976. The control of errors in I.R. spectrophotometry – IV. Corrections for dispersion distortion and the evaluation of both optical constants. Spectrochim. Acta Part A: Mol. Spectrosc. 32, 85–98.

Heitz, T., Drevillon, B., Godet, C., Bouree, J.E., 1998. Quantitative study of C–H bonding in polymer like amorphous carbon films using in situ infrared ellipsometry. Phys. Rev. B – Condens. Matter Mater. Phys. 58, 13957–13973.

Imanaka, H., Smith, M.A., 2007. Role of photoionization in the formation of complex organic molecules in Titan's upper atmosphere. Geophys. Res Lett. 34, L02204. doi:10.1029/2006GL028317.

Imanaka, H., Smith, M.A., 2010. Formation of nitrogenated organic aerosols in the Titan upper atmosphere. Proc. Natl. Acad. Sci. 107, 12423–12428.

Imanaka, H., Khare, B.N., Elsila, J.E., Bakes, E.L.O., McKay, C.P., Cruikshank, D.P., Sugita, S., Matsui, T., Zare, R.N., 2004. Laboratory experiments of Titan tholin formed in cold plasma at various pressures: Implications for nitrogen-containing polycyclic aromatic compounds in Titan haze. Icarus 168, 344–366.

Imanaka, H., Khare, B.N., McKay, C.P., Cruikshank, D.P., 2005. Complex refractive indices of tholins produced from various initial gas mixtures and formation pressures: Implications for Titan, the early Earth, and the outer Solar System bodies. Bull. Am. Astron. Soc. 37, 772–773.

Kersten, R.T., 1975. A new method for measuring refractive index and thickness of liquid and deposited solid thin films. Opt. Commun. 13, 327–329.

Khare, B.N., Sagan, C., Arakawa, E.T., Suits, F., Callcott, T.A., Williams, M.W., 1984. Optical constants of organic tholins produced in a sim- ulated titanian atmosphere: from soft X-ray to microwave frequencies. Icarus 60, 127–137.

Lavvas, P., Yelle, R.V., Griffith, C.A., 2010. Titan's vertical aerosol structure at the Huygens landing site: Constraints on particle size, density, charge, and refractive index. Icarus 210, 832–842.

Lavvas, P., Sander, M., Kraft, M., Imanaka, H., 2011. Surface chemistry and particle shape: Processes for the evolution of aerosols in Titan's atmosphere. Astrophys. J. 728, 80 (11 pp).

Lazar, G., Clin, M., Charvet, S., Therasse, M., Godet, C., Zellama, K., 2003. Effect of the RF power and deposition temperature on the electrical and vibrational properties of carbon nitride films. Diamond Rel. Mater. 12, 201–207.

Lazar, G., Zellama, K., Vascan, I., Stamate, M., Lazar, I., Rusu, I., 2005. Infrared absorption properties of amorphous carbon films. J. Optoelectron. Adv. Mate. 7, 647–652.

Masterson, C.M., Khanna, R.K., 1990. Absorption intensities and complex refractive indices of crystalline HCN, HC_3 N, and C_4 N_2 in the infrared region. Icarus 83, 83–92.

Mayo, L.A., Samuelson, R.E., 2005. Condensate clouds in Titan's north polar stratosphere. Icarus 176, 316–330.

McKay, C.P., Pollcack, J.B., Courtin, R., 1989. The thermal structure of Titan's atmosphere. Icarus 80, 23–53.

McKay, C.P., Pollack, J.B., Courtin, R., 1991. The greenhouse and antigreenhouse effects on Titan. Science 253, 1118–1121.

McKay, C.P. et al., 2001. Physical properties of the organic aerosols and clouds on Titan. Planet. Space Sci. 49, 79–99.

Mennella, V., Brucato, J.R., Colangeli, L., Palumbo, P., 2002. C–H bond formation in carbon grains by exposure to atomic hydrogen: The evolution of the carrier of the interstellar 3.4 micron band. Astrophys. J. 569, 531–540.

Moore, M.H., Ferrante, R.F., Moore, W.J., Hudson, R., 2010. Infrared spectra and optical constants of nitrile ices relevant to Titan's atmosphere. Astrophys. J. Suppl. Ser. 191, 96–112.

Ohta, K., Ishida, H., 1988. Comparison among several numerical integration methods for Kramers–Kronig transformation. Appl. Spectrosc. 42, 952–957.

Palik, E.D. (Ed.), 1991. Handbook of Optical Constants of Solids II. Academic Press, San Diego.

Pearl, J., Ospina, M., Ngoh, M., Khanna, R.K., 1991. Optical constants of solid methane and ethane from 10,000 to 450 cm^{-1}. J. Geophys. Res. 96, 17476–17482.

Quirico, E., Montagnac, G., Lees, V., McMillan, P.F., Szopa, C., Cernogora, G., Rouzaud, J.-N., Simon, P., Bernard, J.-M., Coll, P., Fray, N., Minard, R.D., Raulin, F., Reynard, B., Schmitt, B., 2008. New experimental constraints on the composition and structure of tholins. Icarus 198, 218–231.

Ramirez, S.I., Coll, P., da Silva, A., Navarro-Gonzalez, R., Lafait, J., Raulin, F., 2002. Complex refractive index of Titan's aerosol analogues in the 200–900 nm domain. Icarus 156, 515–529.

Rannou, P., Cours, T., Le Mouelic, S., Rodriguez, S., Sotin, C., Drossart, P., Brown, R., 2010. Titan haze distribution and optical properties retrieved from recent observations. Icarus 208, 850–867.

Ristein, J., Stief, R.T., Ley, L., Beyer, W., 1998. A comparative analysis of a-C:H by infrared spectroscopy and mass selected thermal effusion. J. Appl. Phys. 84, 3836–3847.

Robertson, C.W., Downing, H.D., Curnutte, B., Williams, D., 1975. Optical constants of solid ammonia in the infrared. J. Opt. Soc. Am. 65, 432–435.

Samuelson, R.E., Mayo, L.A., 1991. Thermal infrared properties of Titan's stratospheric aerosol. Icarus 91, 207–219.

Sharda, T., Soga, T., Jimbo, T., 2003. Optical properties of nanocrystalline diamond films by prism coupling technique. J. Appl. Phys. 93, 101–105.

Silva, S.R.P. (Ed.), 2003. Properties of Amorphous Carbon. INSPEC Publication, London.

Soderblom, L.A. et al., 2009. Composition of Titan's surface. Titan Cassini–Huygens, 141–175.

Stenzel, O., Hopfe, V., Klobes, P., 1991. Determination of optical parameters for amorphous thin film materials on semi-transparent substrates from transmittance and reflectance measurements. J. Phys. D 24, 2088–2094.

Swanepoel, R., 1983. Determination of the thickness and optical constants of amorphous silicon. J. Phys. E 16, 1214–1222.

Tanaka, M. et al., 1990. Determination of the infrared proportionality coefficient of the CHn stretching mode for a-C:H and a-SiC:H films using ERD methods. Nucl. Instrum. Method Phys. Res. Sect. B: Beam Interact. Mater. Atoms 45, 223–226.

Tomasko, M.G., West, R.A., 2009. Aerosols in Titan's atmosphere. Titan Cassini–Huygens, 297–321.

Toon, O.B., McKay, C.P., Courtin, R., Ackerman, T.P., 1988. Methane rain on Titan. Icarus 75, 255–284.

Toon, O.B., Tolbert, M.A., Koehler, B.G., Middlebrook, A.M., Jordan, J., 1994. Infrared optical constants of H_2O ice, amorphous nitric acid solutions, and nitric acid hydrates. J. Geophys. Res. 99, 25631–25654.

Tran, B.N., Joseph, J.C., Ferris, J.P., Persans, P.D., Chera, J.J., 2003. Simulation of Titan haze formation using a photochemical flow reactor: The optical constants of the polymer. Icarus 165, 379–390.

Tuntomo, A., Tien, C.L., Park, S.H., 1992. Optical constants of liquid hydrocarbon fuels. Combust. Sci. Technol. 84, 133–140.

Vinatier, S., Bezard, B., de Kok, R., Anderson, C.M., Samuelson, R.E., Nixon, C.A., Mamoutkine, A., Carlson, R.C., Jennings, D.E., Guandique, E.A., Bjoraker, G.L., Flasar, F.M., Kunde, V.G., 2010. Analysis of Cassini/CIRS limb spectra of Titan acquired during the nominal mission II: Aerosol extinction profiles in the 600–1420 cm(−1) spectral range. Icarus 210, 852–866.

Vuitton, V., Tran, B.N., Persans, P.D., Ferris, J.P., 2009. Determination of the complex refractive indices of Titan haze analogs using photothermal deflection spectroscopy. Icarus 203, 663–671.

Waite Jr., J.H. et al., 2007. The process of tholin formation in Titan's upper atmosphere. Science 316, 870–875.

Waite, J.H., Young, D.T., Westlake, J.H., Lunine, J.I., McKay, C.P., Lewis, W.S., 2009. High-altitude production of Titan's aerosols. Titan Cassini–Huygens, 201–214.

Wang, Y., Miyagi, M., 1997. Simultaneous measurement of optical constants of dispersive material at visible and infrared wavelengths. Appl. Opt. 36, 877–884.

Wood, B.E., Roux, J.A., 1982. Infrared optical properties of thin H_2O, NH_3, and CO_2 cryofilms. J. Opt. Soc. Am. 72, 720–728.

Zolotarev, V., Volchek, B., Vlasova, E., 2006. Optical constants of industrial polymers in the IR region. Opt. Spectrosc. 101, 716–723.